

**Blind Deconvolution of Vehicle Inductive Signatures
for Travel Time Estimation**

by

Anushri Parsekar

December 2004

Submitted in partial fulfillment of the

Requirements for the degree of

Master of Science

Under the instruction of Dr. Donald Crouch

Department of Computer Science

University of Minnesota Duluth

Duluth, Minnesota 55812

U. S. A.

UNIVERSITY OF MINNESOTA DULUTH

This is to certify that I have examined this copy of master's thesis by

Anushri Parsekar

And have found that it is completed and satisfactory in all aspects,
and that any and all revisions required by the final examining committee have been made.

Dr. Donald Crouch

Name of Faculty Advisor

Signature of Faculty Advisor

Dr. Taek Kwon

Name of Faculty Co-Advisor

Signature of Faculty Co-Advisor

Date

GRADUATE SCHOOL

ABSTRACT

Travel time provides vital information for traffic monitoring, management and planning. The objective of this thesis is to develop a new computational approach that can measure travel time from two sets of spatially separated loop detectors by a re-identification technique based on vehicle inductance signatures. Past approaches have used the loop inductance signatures, but they only used the features of the raw waveforms ignoring the effect of loss of information by the convolution of the loop system characteristic function, resulting in low re-identification rates.

This thesis proposed a new approach that reverses the effect of convolution by the loop detector in order to separate the original vehicle signatures from the loop output. However, this task is a difficult blind problem since we neither know the impulse response of the loop detector nor the original vehicle signature. To solve this problem, two basic *blind deconvolution* approaches were used in this thesis. The first approach involves estimation of the loop system function based on a speed estimate from the inductance waveform. The estimated loop system function is then used in constructing a Constrained Least Squares (CLS) inverse filter that restores the lost detailed information. The second approach used is an adaptive iterative method referred to as the Godard blind deconvolution. This approach does not require an estimate of the system impulse response, but the outcome depends on the initial condition. We found that the iteration converges to a good solution when the initial condition was set using a CLS filter estimate. According to our experimental results, both methods significantly exposed the original signature information with unique vehicle characteristics. A simple feature extraction technique along with sum of difference coefficients was implemented to test the re-identification rate. The test runs showed high vehicle re-identification rates in comparison to the past research reports. The results obtained are encouraging and suggest that blind deconvolution is an effective technique that can be used for extracting the lost information from the loop system outputs.

ACKNOWLEDGEMENTS

I am grateful to my thesis advisor Dr. Taek Kwon for giving me an opportunity to work under him and for guiding me. I wish to thank him for boosting my confidence with his constant encouragement. Without his support and contribution, this thesis would not have been possible.

I would like to thank my thesis committee members Dr. Donald Crouch and Dr. Carolyn Crouch for their interest in my thesis and their helpful suggestions. I am grateful to David Keranen for his assistance in data collection, to Carol Wolosz from the NATSRL office for her help and to Linda Meek, Lori Lucia, Jim Luttinen and the faculty at Computer Science Department at UMD for their support. Last but not the least, I take this opportunity to thank my family and my friends.

TABLE OF CONTENTS

1. INTRODUCTION.....	1
1.1 MOTIVATION AND OBJECTIVE.....	1
1.2 RELATED WORKS ON TRAVEL TIME.....	2
2. THEORETICAL BACKGROUND	5
2.1 OVERVIEW	5
2.2 DECONVOLUTION.....	6
3 DECONVOLUTION AND BLIND-DECONVOLUTION MODEL FOR VEHICLE REIDENTIFICATION	13
3.1 INDUCTIVE LOOP DETECTOR (ILD) CONVOLUTION MODEL	13
3.2 DECONVOLUTION USING CLS WIENER FILTER	14
3.3 VEHICLE SIGNATURE SEPARATION USING GODARD BLIND DECONVOLUTION TECHNIQUE.....	16
3.4 ILD IMPULSE RESPONSE MODELING	18
4. PROCESSING STEPS FOR TRAVEL TIME COMPUTATION.....	21
4.1 TRAVEL TIME PROCESSING STEPS	21
4.2 ENDPOINT DETECTION	21
4.3 LOW PASS FILTERING AND BLIND DECONVOLUTION	22
4.4 NORMALIZATION	23
4.5 FEATURE EXTRACTION	23
4.6 VEHICLE REIDENTIFICATION	24
4.7 TRAVEL TIME ESTIMATION FOR INDIVIDUAL VEHICLES.....	25
4.8 TRAVEL TIME ESTIMATION FROM GROUP OF VEHICLES	26
5 EXPERIMENTAL RESULTS.....	28
5.1 DATA COLLECTION	28
5.1.1 Highway data.....	28
5.1.2 Data collection for impulse response of loop system.....	29
5.1.3 Waveforms on different speeds of the same vehicle.....	30
5.2 DECONVOLUTION EXAMPLES.....	31
5.2.1 Effect of deconvolution	31
5.2.2 Comparison example of three vehicles in similar length.....	33
5.2.3 Comparison example of three vehicles with the same type.....	34
5.2.4 Reidentification Example-1.....	35
5.2.5 Reidentification Example-2.....	36
5.3 GODARD BLIND DECONVOLUTION EXAMPLES.....	37
5.3.1 Comparison example of three vehicles in similar length.....	37
5.3.2 Comparison example of three passenger car vehicles.....	38
5.3.3 Reidentification Example-1.....	39
5.3.3 Reidentification Example-2.....	40

5.4 SPEED NORMALIZATION	41
5.5 REAL TIME IMPLEMENTATION ASPECTS.....	43
6 CONCLUSIONS AND RECOMMENDATIONS.....	46
6.1 CONCLUSIONS	46
6.2 FUTURE RECOMMENDATIONS	46
REFERENCES.....	48

LIST OF TABLES

Table 1: Vehicle length estimates based on peaks of waveform	19
Table 2: Performance results of the 3M test data	44
Table 3: Re-identification rates for the 3M test data with threshold on the difference coefficient	45

LIST OF FIGURES

Figure 1: Inductance waveform of a typical passenger vehicle. Horizontal axis intervals are in 10 milliseconds.	6
Figure 2: Block diagram illustrating convolution and deconvolution process for vehicle signature extraction.	7
Figure 3: Adaptation using Bussgang type algorithms	8
Figure 4: Godard Deconvolution	16
Figure 5: Estimated loop model of a semi-truck with 66ft of length traveling at 40 mph	20
Figure 6: Travel time computational steps.....	21
Figure 7: Data collection equipment: left=detector cabinet, right=laptop computers	28
Figure 8: Video recording system with loop actuation and timestamp	29
Figure 9: Apparatus used for loop system impulse response.....	29
Figure 10: Ford Ranger used to collect inductance waveforms at various speeds	30
Figure 11: Inductance waveform of two passenger vehicles recorded in two separate stations	31
Figure 12: Result of deconvolution.....	32
Figure 13: Comparison of vehicle with a similar length.....	33
Figure 14: Comparison of three passenger car vehicles: before deconvolution=solid line, after deconvolution=dotted line	34
Figure 15: Vehicle reidentification. (a) is the upstream vehicle, and (b)-(d) are possible match candidates at the downstream vehicles. (Before deconvolution=solid, after deconvolution=dotted).	35
Figure 16: Vehicle reidentification. (a) is the upstream vehicle, and (b)-(d) are possible match candidates at the downstream vehicles. (Before deconvolution=solid, after deconvolution=dotted).	36
Figure 17: Comparison of vehicle waveforms with a similar length before and after Godard blind deconvolution. The three vehicles are a car, a van, and a pick-up truck.	37
Figure 18: Comparison of three passenger car vehicles on before and after deconvolution: before=solid, after=dotted.....	38
Figure 19: Vehicle reidentification. (a) is the upstream vehicle, and (b)-(d) are possible match candidates at the downstream vehicles. (Before deconvolution=solid, after deconvolution=dotted).	39

Figure 20: Vehicle reidentification. (a) is the upstream vehicle, and (b)-(d) are possible match candidates at the downstream vehicles. (Before deconvolution=solid, after deconvolution=dotted). 40

Figure 21: Original (dotted) and deconvolved and then resampled (solid) signature of Ford Ranger driven at 10mph 41

Figure 22: Original (dotted) and deconvolved (solid) signature of Ford Ranger driven at 39mph. 41

Figure 23: Speed normalization down-sampling 43

1. INTRODUCTION

1.1 Motivation and Objective

Travel time provides vital information for traffic monitoring, management and planning. It serves transportation decision makers in evaluating the efficacy of traffic networks as well as the performance of traffic management strategies. It is an important variable in developing real-time route guidance systems since travel time is considered more informative to motorists than local velocity measurements. The accuracy of such guidance systems depends on reliable and timely travel time measurements. Our main interest in this thesis is to devise a method for measuring travel time for a section of highways. The dynamic route travel time can then be always computed by adding real time measurement of section travel times.

Direct measurement of travel time is difficult and costly, as it requires new communication infrastructure and people/vehicle coordination. The approach in this thesis solves the real time estimation of travel time using signal analysis of the existing loop detectors. Since many highways already have sufficient installed bases of inductive loop detectors (ILDs), it is a more cost-effective solution to measure the travel time.

The data obtained from ILDs is in the form of traffic volume and occupancy of the road in a preset time interval. In the past, many traffic parameters such as speed, density, travel time and congestion indices were estimated using these two parameters (Mikhalkin, 1972). However, accuracy has been unsatisfactory, mainly due to the limitation that vehicle length and speed information cannot be reliably derived from the volume and occupancy information. In order to alleviate this problem, a set of double loops referred to as a speed trap configuration has been used. This approach provides speed data from which vehicle length data can be derived. However, it also significantly increases the cost of installation and maintenance.

The objective of this research is to advance the new technology of measuring travel-time of freeway sections using inductance signatures of vehicles that are generated by loop detectors. In the prior approaches of utilizing inductive signal analysis, vehicle

waveforms were directly used for vehicle identifications. Such approaches have shown limitations in identification rates due to the loss of details of vehicle characteristics on the waveform affected by the moving average of loop inductance. This research focuses on restoring the loss of information through a class of methods referred to as deconvolution and blind deconvolution.

1.2 Related Works On Travel Time

Travel time can be obtained in a number of ways. They can be measured directly using probing vehicles or by advanced detection technologies (e.g., AVI, AVL, and video image processing), or estimated indirectly from volume and occupancy traffic data. However, each method has its own drawbacks, and it is still considered an open research area. Estimating speeds using volume and occupancy relationships of loop data and converting them into travel time has been proposed by numerous researchers (Dailey, 1999; Mikhalkin, 1972; Pushkar, 1994; Coifman, 2000), but the limitation in their accuracy under delayed conditions (e.g., incidents and congestions) has been widely observed.

Recently, measurements of travel-time have been increasingly viewed as an important issue in traffic monitoring and management. As a result, several pioneering research projects have been proposed and are under way. In the California PATH program (Tam 1999/2000), Yim et al. (2000) have been studying the use of cell phones to probe the GPS units in selected vehicles for travel time estimation. MacCarley and Obispo (Tam 1999/2000) proposed the use of video based signature analysis in which vehicle tracking is accomplished using the analysis of video images. Harry proposed the use of a real-time laser-based detection system for speed from which it is converted into travel time measurements (Tam 1999/2000).

In another direction, researchers began to focus on improving the old technologies such as loop detectors. The data obtained from the conventional loop detectors is digital in the form of pulses indicating the presence of a vehicle over the loop. New inductive loop detectors began to provide the waveforms of inductance changes as a vehicle passes over the loop. The shape of this inductance waveform depends on various factors such as the length of the vehicle, speed of the vehicle, the material with which the vehicle is

made, the height of the vehicle from the road, etc. Since the inductive loop waveforms can provide considerable amount of information about the vehicle, numerous new applications of loop detectors began to emerge such as vehicle classification and single-loop speed measurement (Sun & Ritchie, 1999, Sun, 2000).

Sun (2000) proposed two different classification methods that utilize inductance waveforms to classify vehicles into seven predefined vehicle classes. The first method uses a Self-Organizing Feature Map (SOFM), which is a well-known artificial neural network approach that has been used in pattern classifications. The second method uses a heuristic discriminant algorithm to classify the vehicles. The inputs to this algorithm are feature vectors obtained by processing the inductive loop waveforms. The feature vectors include the length, signature variance, skewness, kurtosis, and Discrete Fourier Transform (DFT) coefficients (Sun 2000).

Another study by Sun and Ritchie (1999) describes the use of single inductive loop signature for the estimation of individual vehicle speed. This method makes a use of the fact that speed of a vehicle is correlated to the slew rate of the inductive loop waveform where the slew rate is the rate of change in inductance. The algorithm calculates the slew rate by extracting the leading and trailing edges of the inductance waveform by finding the local maxima. The speed is then estimated using a linear regression method. These approaches are in initial research states, and further study is needed to increase the accuracy.

As opposed to the above approaches, vehicle travel time can also be estimated by using a pair of loop stations (upstream station and downstream station). In this approach, the speed is calculated from the time it takes for the vehicle to travel from the first loop to the second loop. However, this requires reidentification of the same vehicle by matching the vehicle signature at the second loop. The problem of reidentification of the vehicle can be tackled in several ways. One algorithm proposed by Sun et al. (2002) identifies the upstream origin of the vehicle based on either a heuristic method or a probabilistic neural network (PNN) method. The algorithm filters individual vehicle turning movements to identify the upstream origin more accurately.

Another methodology is to extract the features of the inductance signatures generated by each vehicle passing through the upstream station and then to re-identify

them at the downstream station by matching the features from the upstream end. In order to obtain high re-identification rates it is important to be able to extract detailed features from the signatures, which will act as discrimination factors in re-identification of vehicles.

In the above-mentioned approaches (Sun's and others), inductance outputs of loop detectors were directly used for vehicle identification (Sun, 2000). Such approaches have inherent limitation in identification rates, since the loop detector outputs are generated as a moving average of inductances with the window size determined by the loop length (typically 6 feet).

A new approach that this thesis pursued is to separate the raw inductance output into speed component, loop signal, and the vehicle signal by using a class of techniques called blind deconvolution (also called blind separation for multiple inputs). We demonstrate that tracing back the original signal source of vehicles provides more unique signatures from which a higher identification rate is achievable.

2. THEORETICAL BACKGROUND

2.1 Inductive Waveform

Inductive loop detectors (ILDs) consist of one or more loops of wire embedded in the pavement and connected to a control box, excited by a signal ranging from 10KHz to 200 KHz. ILDs are essentially a resonance circuit and operate on the principle of electromagnetic inductance and capacitance. The wire loop excited with a frequency signal functions as an inductive element and the capacitance is provided by the capacitors embedded in the detector card. An alternative current is constantly applied to the loop circuit to maintain a constant level of inductance at the loop. As a vehicle passes through the loop, the inductance is reduced due to the eddy currents formed on the surface of the metal portion of the vehicle. This reduction of inductance in the resonance circuit results in increasing the resonance frequency of the loop detector. This relation is given by:

$$\text{Resonance frequency} = \frac{1}{2 \times \pi \times \sqrt{L \times C}} \quad (1)$$

where L is inductance and C is capacitance of the loop. Loop detectors typically detect this frequency changes by zero-cross counting. The frequency increase is then computed back to inductance changes. The change in inductance due to the presence of a vehicle is recorded at a small time-interval. The waveform obtained by plotting the sampled inductance changes is referred to as the *vehicle inductive waveform* or *inductance signature*. This waveform depends on a number of vehicle parameters such as the vehicle length, speed, metal surface, etc. Figure 1 shows an inductive waveform of a typical passenger car. Horizontal axis is recording of data points at 10 milliseconds interval.

In the past approaches, raw inductance waveforms as shown in Figure 1 have been directly used to extract vehicle features (Sun, 2000). Since most ILD sensing zone is large enough to cover a single lane width, the inductance outputs are not the detailed features of the vehicle but a moving average of the inductance changes caused by the overlapped area between the loop and the vehicle. Consequently, many details are already lost by the summing effect, and it is hard to extract distinctive features from the raw inductance data generated by ILD. This is evident by a common shape of inductance

waveform that has one peak in the middle with monotonic decrease in both sides as shown in Figure 1.

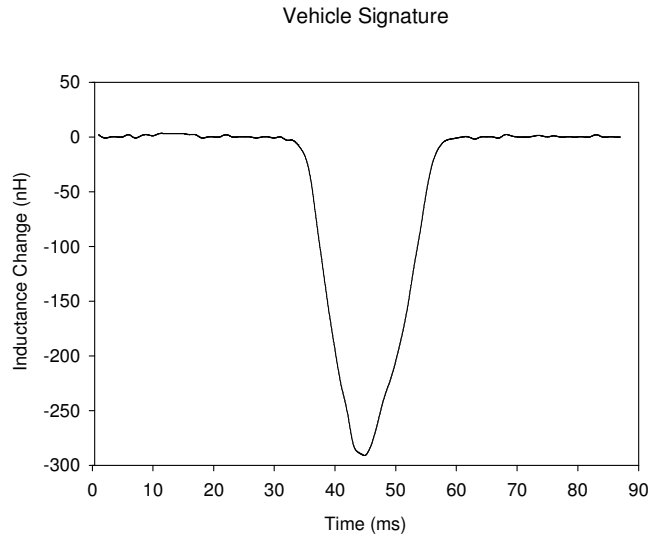


Figure 1: Inductance waveform of a typical passenger vehicle. Horizontal axis intervals are in 10 milliseconds.

2.2 Deconvolution

As a system point of view, the output of the detector card could be considered as a convolution of inductance signature of the vehicle and the loop characteristic function. According to the observation of waveforms generated, the differences among the vehicles in the same class are minute in their inductive patterns. This similarity effect is clearly caused by the convolution of the inputs by the loop system function which smoothes out the discriminating features of individual vehicles. For matching the vehicles by comparing vehicle inductive waveforms, it is much more effective to use the original vehicle characteristic than the convolved waveform. Hence, we must find inputs knowing only the output of the convolution. This type of problem is referred to as a blind problem and a class of techniques used to solve this problem is referred to as *blind deconvolution*, which essentially attempts to reconstruct the input signal from the output signal without knowing both the input signal and the system.

The objective of the blind de-convolution in the feature extraction process is to find the inverse system that discriminates vehicle signatures as shown in Figure 2. Since we do not know the vehicle shapes and loop conditions from the available inductance output, this process is clearly a blind operation.

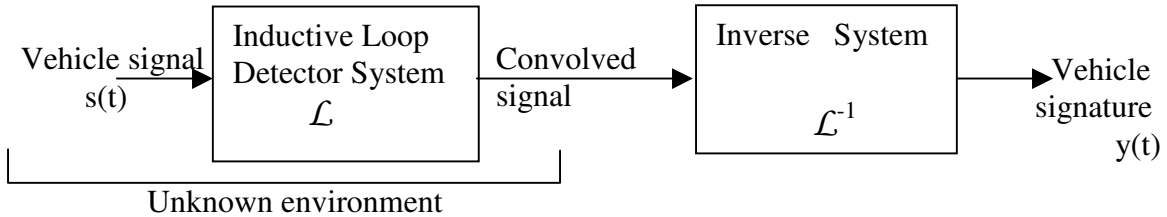


Figure 2: Block diagram illustrating convolution and deconvolution process for vehicle signature extraction.

The techniques used for blind deconvolution are similar to the ones used for blind channel-equalization. The need for channel-equalization arises from the fact that during signal communication, the channel through which data is transmitted usually distorts the original signal. In channel-equalization, the convolution effects of the channel are cancelled from the received signal using interference cancellation techniques. Among the first few developed techniques for blind channel equalization are the decision-directed mode of operating the least-mean-square algorithm and the Sato algorithm. A paper by Lucky (1966) describes the decision-directed (DD) algorithm for blind channel-equalization. The Sato algorithm (Sato, 1975) in 1975 was motivated by the fact that the DD algorithm failed to readapt to a newly connected channel. Godard (1980) made another important contribution when he proposed the Godard class of algorithms for blind channel-equalization. Many of the blind deconvolution techniques developed today have their roots in the blind channel-equalization methods.

One way to achieve blind deconvolution is by unsupervised adaptive filtering. Adaptive filtering is a form of recursive filtering in which the filter parameters are adjusted until the desired output is obtained. Adaptive filtering is termed as unsupervised when the filter parameters are adjusted without having the desired response of the filter. However, even for the unsupervised, the filter parameters are adjusted according to a set

of rules, which allows the filter to calculate a desirable input to output mapping. There are three fundamental approaches to unsupervised adaptive filtering:

1. Bussgang Statistics
2. Higher order statistics
3. Information-Theoretic models

A Bussgang process has the property that its autocorrelation function is equal to the cross-correlation between the process and the output of a zero-memory non-linearity produced by that process (Haykin, 2000). Hence, for a Bussgang process the output follows a condition given by:

$$E[y(t)y(t-k)] \approx E[y(t)g(y(t-k))] \quad (2)$$

where $g(\cdot)$ represents a non-linearity.

Unsupervised adaptive filters that satisfy this condition are classified as Bussgang algorithms. These include the DD algorithm, Sato algorithm and the constant-modulus algorithm (CMA) (Haykin, 2000). A block diagram of an unsupervised adaptive filter of the Bussgang type is shown in Figure 3 (Haykin, 2000).

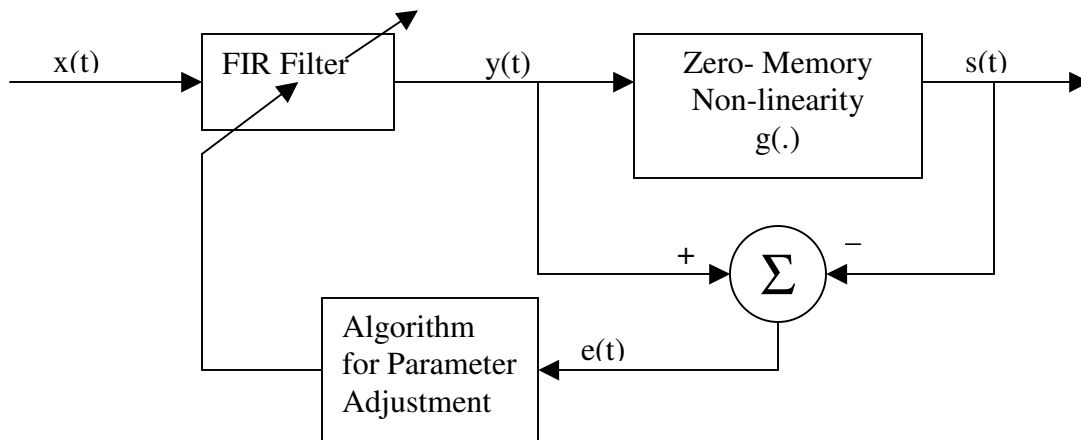


Figure 3: Adaptation using Bussgang type algorithms

The input $x(t)$ is the distorted signal received. The aim is to design a FIR filter that can recover the original signal from $x(t)$ without knowing the transfer function of the distorting system. The parameters of the FIR filter are recursively adjusted until it gives

close approximation to the inverse of the transfer function that has distorted the output. The output of the zero memory non-linearity acts as the estimated original signal $s(t)$, and $e(t)$ is the error or difference between the output of the filter and the estimated signal.

Busgang algorithms have been used widely for blind equalization of communication channels. A paper by Nowlan and Hinton (1993) describes a soft decision-directed least-mean-square algorithm that converges in channels where the conventional DD algorithm fails to converge. Another work by Weerackody et al. (1994) uses the Sato algorithm and the Godard algorithm for initial convergence but switches to the DD algorithm when the error has a very small value. This is because both the Sato algorithm and the Godard algorithm have a slow convergence rate. The constant modulus algorithm was the most studied and implemented algorithm for blind equalization in the 1990s (Johnson et al., 1998). However the choice of the algorithm to use depends on the communication system used, the convergence rate required and the residual error after convergence (Lee & Cheun, 1999).

All these approaches were developed to recover digital communication signals but fail to perform well when applied to impulsive signals (Mathis & Douglas, 1999). Mathis & Douglas (1999) provided a theoretical and analytical explanation as to why the conventional Busgang algorithms are unsuitable for impulsive signals. Their work discusses a modified Sato algorithm, which can be used for impulsive signals such as acoustic signals in seismic and audio signal processing. Nokas et al (1998) proposed to use blind deconvolution to deconvolve the speech signals that contain the impulse response of the surrounding and the impulse response of the transducer. In their approach the CMA algorithm was used for adaptive deconvolution and a higher order statistical blind deconvolution method was used to estimate the impulse response of the room.

The second type of blind deconvolution approaches makes an explicit use of the higher order statistics of the observed signal. The higher-order statistics of a stationary process are described in terms of cumulants (generalization of autocorrelation function) and their Fourier transforms known as polyspectra (generalization of power spectrum) (Haykin, 2000). The Higher order statistics (HOS) approaches attempt to estimate the impulse response, $h[n]$ of the distorting system (system identification) by using information hidden in the cumulants (Olofsson, 1996) . Higher order (>2) cumulants

contain not only the amplitude but also phase information of the unknown system (Feng & Chi, 1999) as opposed to autocorrelation function, which does not preserve the phase information of a signal. Another added advantage of using higher order cumulants is that they are insensitive to Gaussian noise. However higher order statistics are applicable when dealing with non-Gaussian processes (Feng & Chi, 1999). Fortunately, many real world applications are truly non-Gaussian (Feng & Chi, 1999). Another important factor that has to be considered while estimating the impulse response, $h[n]$, is whether the system is a minimum phase system or not. Other methods such as the prediction error method (PEM) are known to have problems for identifying non-minimum phase systems (Olofsson, 1996). However, higher order cumulant approaches can be used in estimating impulse response for a non-minimum phase system.

High Order Cumulants based techniques can be classified into two categories: non-parametric methods and parametric methods. The non-parametric methods are Fourier based and work in the frequency domain, but are not popularly used (Mendel, 1991). The parametric methods first estimate the parameters of the system generating the output and then use it to compute the polyspectrum (Feng & Chi, 1999). These methods provide results with higher resolution and lower variance and hence are preferred over the non-parametric ones (Zheng et al., 1991). Most parametric methods use second order, third order, fourth order or a combination of these ordered cumulants. Olofsson et. al. (1996) compared the results obtained from the Higher Order Cumulant Method with the classical PEM along with two other methods (Nowlan & Hinton, 1993). They also presented results to illustrate the capability to identify minimum and non-minimum-phase systems. Another study by Feng and Chi (1999) proposed an inverse filter criterion for optimum inverse filter design using joint cumulants. This method attempts to optimize $v(n)$, an estimate of $h[n]$ by maximizing $J_{r,m}(v(n))$ given by:

$$J_{r,m}(v(n)) = \frac{|C_m\{e(n)\}|^r}{|C_r\{e(n)\}|^m} \quad (3)$$

where,

$$r \text{ is even, } m > r \geq 2,$$

$C_m\{e(n)\}$ and $C_r\{e(n)\}$ denote the m -th order and r -th order cumulants of $e(n)$, respectively (Feng & Chi, 1999).

Here $J_{r,m}(v(n))$ is the inverse filter criterion that is to be maximized to obtain the optimum inverse filter $h[n]$. This method is actually based on the criteria for blind deconvolution of non-minimum phase channels, which were proposed, by Shalvi and Weinstein (1990) for communication channels. A similar algorithm based on third and fourth order cumulants was proposed by Zheng et al. (1991) for blind deconvolution and identification of non-minimum phase systems. However, this algorithm makes use of only the diagonal cumulants, which makes it simpler. It reduces the problem of blind deconvolution to solving a set of linear equations. Higher order cumulant based techniques form a significant part of blind deconvolution.

Another class of techniques used for blind deconvolution is based on information-theoretic models. These techniques use the concepts from Shannon's information theory, namely, entropy and mutual information (Haykin, 2000). The entropy of a process defined as the amount of information in that process. It is actually a measure of self-information (information about the process itself). Another important notion is that of mutual information. Mutual information refers to the information contained in one process about another process.

Let a source of information be denoted by the vector x and let vector y be the output of a system produced in response to the vector x , then the differential entropy $h(X)$ of the source is obtained as:

$$\begin{aligned} h(X) &= -E[\log f(x)] \\ &= -\int_{-\infty}^{\infty} f(x) \log f(x) dx \end{aligned} \quad (4)$$

Let the mutual information be denoted $I(X;Y)$, then it is calculated as:

$$\begin{aligned} I(X;Y) &= h(X) - h(X/Y) \\ &= -\int_{-\infty}^{\infty} \int_{-\infty}^{\infty} f(x, y) \log \left(\frac{f(x/y)}{f(x)} \right) \end{aligned} \quad (5)$$

Looking at Eq. (5) the mutual information can be interpreted as the information contained in one process minus the information contained in the process when the other process is known (Gray, 1990). A study by Bell and Sejonowski (1995) devised

maximization of the differential entropy for blind source separation. The problem of reversing the convolution is constructed as a maximization of the entropy $H(y)$ of a non-linearly transformed signal $y = g(x)$ where g is some function and x is the input. This algorithm is relatively new but has the advantage of being simple yet effective (Haykin, 2000).

The three classes namely Busgang Statistics, higher order statistics and information theoretic models are the main techniques in blind deconvolution using unsupervised adaptive filtering. The approach for solving the problem of blind deconvolution of the inductance loop signature applied in this these involves starting with a rough approximation of the loop model filter and then adjusting its coefficients using the Godard blind deconvolution technique.

3 DECONVOLUTION AND BLIND-DECONVOLUTION MODEL FOR VEHICLE REIDENTIFICATION

3.1 Inductive Loop Detector (ILD) Convolution Model

From a system point of view, inductance signature of a vehicle can be considered as a convolved signal between the vehicle signal and the loop system as shown in Figure 2. ILD is essentially similar to an averaging filter since the loop typically covers an area (detection zone of a 6'x6' loop is about 8'x8') in which the vehicle is present. Consequently, many details of the vehicle characteristics are lost. In order to recover the lost information, an inverse filter is needed as it was shown in Figure 2. Computing an estimate of the original vehicle signal using an inverse system is referred to as a deconvolution.

The objective of deconvolution is to extract vehicle signatures out of the convolved output of ILD. As in any signal system, noise would be contained in the output. Since the system output is produced by an electrical system, the noise is modeled as Gaussian random noise. Including the noise effect, we model the output of an ILD system as follows:

$$g = Hf + n \quad (6)$$

where g , f and n are M -dimensional column vectors that denote ILD output, true vehicle signature, and Gaussian random noise, respectively. The column vectors are:

$$g = \begin{pmatrix} g(0) \\ g(1) \\ \vdots \\ g(M-1) \end{pmatrix}, \quad (7)$$

$$f = \begin{pmatrix} f(0) \\ f(1) \\ \vdots \\ f(M-1) \end{pmatrix}, \quad (8)$$

and

$$n = \begin{pmatrix} n(0) \\ n(1) \\ \vdots \\ n(M-1) \end{pmatrix}. \quad (9)$$

Each component of the column vectors in Eqs. (7), (8), and (9) corresponds to the digital sequence of the original analog values. The ILD system, H is an $M \times M$ matrix and expressed by a circular shift of the rows to the right, i.e.,

$$H = \begin{pmatrix} h(0) & h(M-1) & h(M-2) & \dots & h(1) \\ h(1) & h(0) & h(M-1) & \dots & h(2) \\ h(2) & h(1) & h(0) & \dots & h(3) \\ \vdots & \vdots & \vdots & & \vdots \\ h(M-1) & h(M-2) & h(M-3) & \dots & h(0) \end{pmatrix} \quad (10)$$

A square matrix in which each row is a circular shift of the preceding row, and the first row is a circular shift of the last row, is called a circulant matrix and commonly used for modeling convolution (Gonzalez & Woods, 1993). It is also called a channel convolution matrix (Haykin, 2000).

3.2 Deconvolution using CLS Wiener filter

The only known and available value in Eq. (6) is the ILD inductance output g . However, the circulant matrix H could also be obtained from an impulse response of the ILD system. A number of methods in estimating impulse response will be discussed in Section 5.4. Thus, our objective is now finding f given g and H . First, we introduce a cost function J given by,

$$J(f) = \frac{1}{2} \| g - H * f \|^2 \quad (11)$$

Eq. (11) is called a *least squares* cost function (Gonzalez & Woods, 1993), and the task is reduced to finding f that minimizes the cost function. Differentiating J with respect to f and setting the resulting vector equal to a zero vector gives,

$$-H^T (g - Hf) = 0 \quad (12)$$

Solving Eq. (12) for f yields,

$$\hat{f} = \frac{H^T g}{(H^T H)^{-1}} \quad (13)$$

In Eq. (13), an estimation notation \hat{f} was used since it is a solution of minimization. This solution tends to be unstable when H contains singular values. A more stable approach called regularization can be established using the following cost function.

$$J(f) = \frac{1}{2} (\|g - H\hat{f}\|^2 - \|n\|^2) + \frac{1}{2} \alpha \|Qf\|^2 \quad (14)$$

where α is called a regularization parameter and Q is a linear operator that works as a stabilizer. Since the second term in Eq. (14) works as a constraint, this approach is referred to as the Constrained Least Squares (CLS) filter. Characteristics of CLS filters in robustness were extensively studied by Zervakis & Kwon (1993).

To find the minimum of the cost function $J(f)$, we let its derivative to zero.

$$\frac{\partial J(f)}{\partial f} = 0 \quad (15)$$

Solving Eq. (15), the estimate of the vehicle signature \hat{f} is now written as,

$$\hat{f} = \frac{H^T g}{H^T H + \alpha Q^* Q} \quad (16)$$

The linear operator Q is implemented as a high pass filter. This type of inverse filter is commonly used in signal processing (Gonzalez & Woods, 1993, Haykin, 2000).

3.3 Vehicle Signature Separation using Godard Blind Deconvolution Technique

The inverse filter in Eq. (16) is used with an estimate of impulse response of the loop system H . In communication channels, impulse response is easily estimated using pilot impulse signals during the initial learning phase. In an ILD system, since the impulse input must be a form of physical system that moves over the loop, it is not easy to obtain. More specifically, it is difficult to generate an impulse input since we do not know what constitutes the impulse input of the loop system. Thus, the problem of finding the vehicle signature is a true blind deconvolution problem. Figure 4 illustrates the Godard blind-deconvolution process in which a rough system estimate can be used. The inverse system W is selected as a rough initial estimate of the ILD system function H . In this thesis, we use a simplified modeling (discussed in Section 3.4) to obtain the ILD system function, and the inverse is chosen using Eq. (16). The Godard blind deconvolution is then applied through iterative steps using the Godard error function in order to adjust the coefficients of W . Godard (1980) has already proven that this iteration converges given that the iteration rates are properly selected.

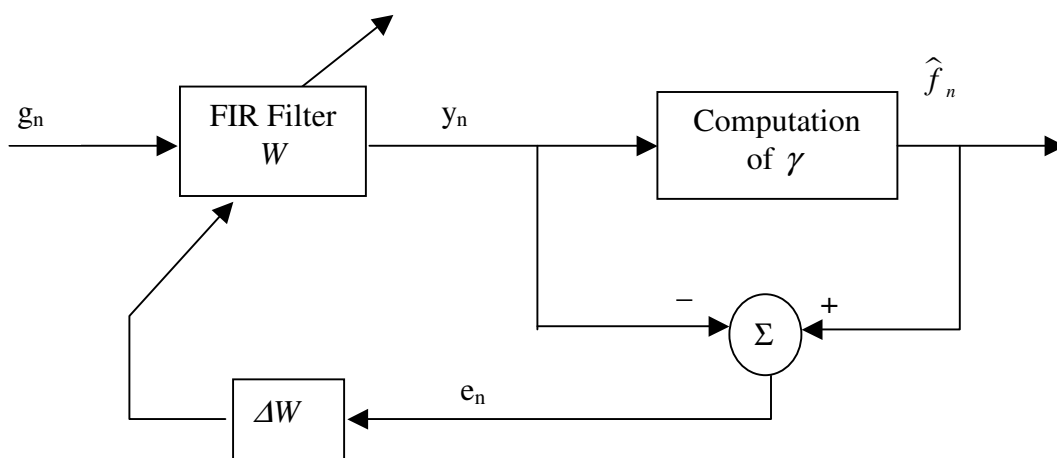


Figure 4: Godard Deconvolution

From Figure 4, an estimate of the true signature denoted by y is computed as the convolution of the ILD output g with an estimated inverse system W with M parameters.

$$y = gW \quad (17)$$

where y and g are M -dimensional column vectors, and W is an $M \times M$ block circulant

matrix. Using statistical properties of y , the nonlinearity γ in Godard blind deconvolution, is chosen as below

$$\gamma = \frac{E[|y_n|^4]}{E[|y_n|^2]} \quad (18)$$

or equivalently,

$$\gamma = \frac{E[|y_n|^4]}{\sigma_y^2} \quad (19)$$

The Godard criterion is then written as

$$J = \frac{1}{4} E\{|y_n|^2 - \gamma\}^2 \quad (20)$$

The amount of error ΔW is computed by minimizing this criterion and is obtained as:

$$\Delta W = y_n(\gamma - y_n^2) \quad (21)$$

The inverse filter coefficients for the new iteration are then calculated as follows,

$$W(k) = W(k) + \eta \Delta W g(k - M - 1) \quad (22)$$

where η is an iteration rate that is selected depending on the statistical condition of output y_n to make the system converge.

At the end of the iterations the inverse filter W obtained is close to the inverse of ILD system. It is then used to get the final output by convolving it with the ILD output to retrieve the true signature, i.e.,

$$\hat{f} = gW \quad (23)$$

Notice that the final outcome shown in Eq. (23) only involves the knowledge of the observed vehicle waveform. Since it is computed without the knowledge of the system, this operation is referred to as a blind operation.

For actual implementation, the algorithm is implemented in Discrete Fourier Transform (DFT) domain. The final output is then converted back into discrete time domain.

3.4 ILD Impulse Response Modeling

As discussed in the previous sections, we do not need to know the precise impulse response of the ILD system to successfully extract the vehicle signatures, but a reasonable estimate that can be used as a starting point of the blind deconvolution iteration. This section discusses how to obtain the initial estimation.

The shape of the loop impulse response can be modeled by considering the amount of flux produced by the loop over its area of 6x6 ft. The flux produced by the loop increases from the edge, reaches a peak plateau, and then decreases towards the other edge. The duration for which a vehicle significantly affects the loop flux is the time needed for a vehicle to pass over the loop. This duration depends on the speed of the vehicle as well as the length of the vehicle. Thus, the length of the loop impulse response can be modeled for each vehicle as a function of its speed and the time it will take to pass over the 6 ft loop. To achieve this it is necessary to estimate the speed of the vehicle from a single loop signature. The length of the signature gives the time needed for the vehicle to cover a distance of 6 ft in addition to the vehicle's length itself. Using estimated lengths of vehicles, the speed can be estimated as

$$Speed = \frac{(6 + length) \times 0.6818}{sig_len} \quad (24)$$

where, $Speed$ = estimated vehicle speed in miles per hour

$length$ = estimated length of the vehicle

sig_len = length of the inductance signature

If the same average length is used for all vehicles irrespective of whether it is a passenger car or a long truck, then it leads to speed underestimates for longer vehicles and speed overestimates for shorter vehicles. To solve this problem, the vehicles lengths are assigned using basic features of the inductance waveform. The number of peaks in the signature is the main feature used to classify the vehicle and assign the estimated vehicle length. Table 1 shows the number of peaks, the possible vehicle type and the length used for estimating the speed.

Table 1: Vehicle length estimates based on peaks of waveform

No. of Peaks in the signature	Possible Vehicle Type	Length (in feet)
1	Passenger car/ van	21
2	Pickup truck	23
3	Delivery truck/ van	30
4	Truck	40
5	Semi trailer truck	58
>=6	Long truck with trailers	66

Once the vehicle length is estimated from the inductance signature, the speed of the vehicle is estimated using Eq. 24. Using this speed estimate, the length of the loop model can be calculated from the time it would take the vehicle to travel 6 ft. Higher the estimated speed smaller is the length of the loop model since the vehicle passes quickly over the loop. Although the length of the loop model depends on the speed of the vehicle the overall shape remains the same and is modeled by using the cumulative distribution function for a Gaussian function. The loop model is assumed to be symmetrical and one half of that is estimated using:

$$H(x) = \sum_{i=0}^x \frac{1}{\sigma\sqrt{2\pi}} e^{-\frac{(i-\mu)^2}{2\sigma^2}} \quad (25)$$

where, μ = mean of the Gaussian function

σ^2 = variance of the Gaussian function

The mean and the variance of the Gaussian are manipulated to obtain the required length of the loop model and they do not have any statistical significance. Figure 5 shows an example of the estimated loop model for a truck with length 66 ft traveling at a speed of 40 miles/hr.

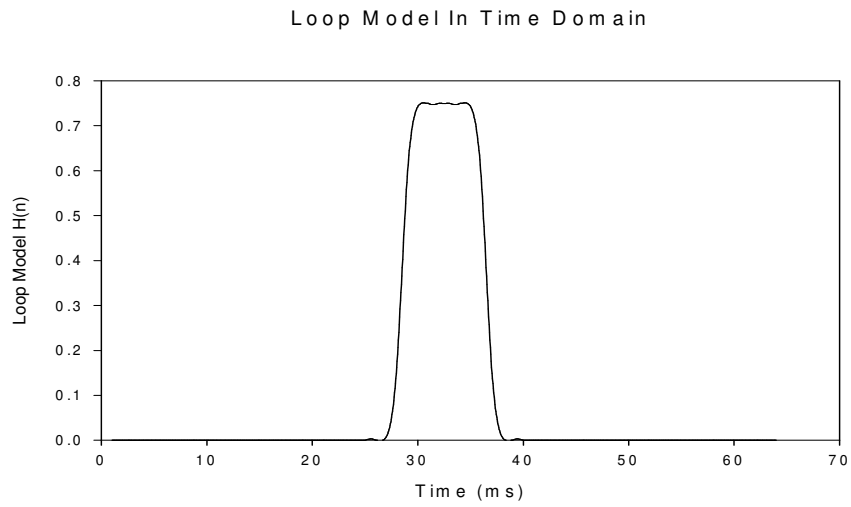


Figure 5: Estimated loop model of a semi-truck with 66ft of length traveling at 40 mph

4. PROCESSING STEPS FOR TRAVEL TIME COMPUTATION

4.1 Travel Time Processing Steps

The processing steps for travel time computation can be implemented as a sequence of modularized steps. Figure 6 shows the series of steps that are required to process from the raw inductance data.

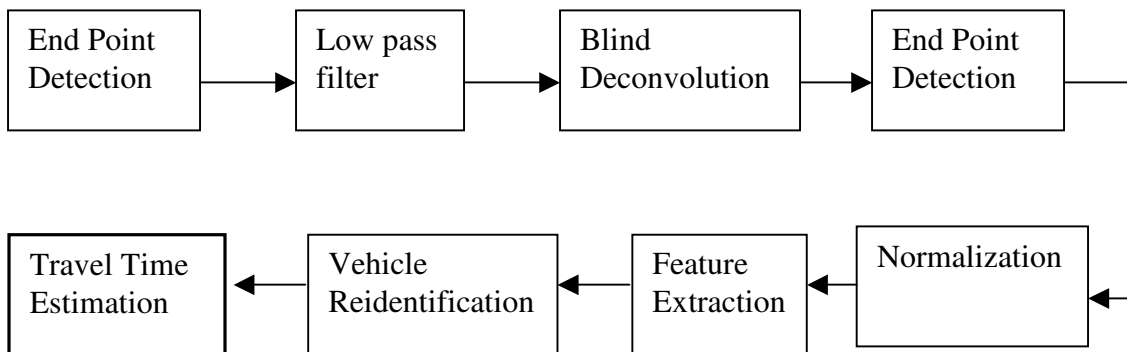


Figure 6: Travel time computational steps

Each of the steps is described in detail along with the method of implementation, the related problems, and their solutions.

4.2 Endpoint Detection

Since the raw data received from an ILD card is a continuous stream of sampled inductance data stream, the very first step before analyzing the waveforms is to identify the beginning and ending of the vehicle waveform. This process removes data recorded during the idle state and enables us to pass the vehicle waveforms to the next processing step. This process is referred to as the endpoint detection.

A number of methods can be used for endpoint detection. A simplest method is to check for zero crossing but it frequently fails due to the presence of noise. Another method would be to check when the channel signal crosses a certain threshold, but this approach also has its own problems. A proper threshold level depends on the noise characteristics and it is difficult to determine which level is optimal. If the threshold is

selected too low then there can be false threshold crossing due to noise. If the threshold is too high, then the start of the vehicle signature may be located well before the point where the channel signal crosses the threshold.

The algorithm used in this thesis it to utilize the slope of the channel signal along with a rough cut by a relatively high threshold. The algorithm works as follows. First, the threshold method is used to crudely determine the start and end of the signature by setting the threshold level well above the channel idle noise level. This ensures not detecting noise as a vehicle. Second, using the slope of the waveform the starting and ending points are extended until the absolute value of slope is reduced by a certain percent (typically 40% or more).

4.3 Low Pass Filtering and Blind Deconvolution

The next step is to implement the deconvolution techniques described in Section 3. To make this task simple it is desirable that all the signals are first converted to the frequency domain (DFT). First, the complete channel signal is divided into segments of size N each (where N can be chosen from 256, 512, or 1024) and then each segment is converted to the frequency domain using N -point FFT (Fast Fourier Transform). However, this method leads to a problem of ringing due to the Gibbs phenomenon when the vehicle signature is partly in one segment and partly in another. To rectify this problem, individual signatures are segmented out using the endpoint detection data, and shifted so that the entire signature lies in the N -point segment. However, segmenting out the individual vehicle waveforms leads to an increase in the high frequency components, which introduces another undesirable ringing effect during the inverse filtering process. Therefore, to smoothen out the effect of sharp segment of the waveform, individual signatures are low pass filtered. A linear phase low pass filter with cutoff frequency of 0.5 with order 32 is designed and used for this purpose.

The individual waveforms are processed using the techniques described in Section 3, i.e., Eqs. (16) and (23). After obtaining the deconvolved signatures, endpoint detection is carried out once again to find the start and end of the processed signatures.

4.4 Normalization

The task of signature matching is simplified by deconvolution. However, few basic issues need to be addressed to achieve accurate matching. The first issue is that amplitude or height of the vehicle signature varies from one loop to another even if the vehicle is the same one. This is predictable since the vehicle may not pass the loops the same way and some differences will always exist between any two loop installations. Hence, some kind of amplitude normalization is required. However, we cannot scale all of the signatures to the same amplitude since it would destroy the information about the height of the vehicles. To achieve both i.e. keep intact the height information of individual vehicles and still have a common ground for comparing the vehicle signatures of the same vehicle for different channels (each loop data is obtained from a single channel of the detector card), a channel amplitude normalization approach was used as follows. The maximum for each deconvolved channel signal is calculated and then dividing it by this channel maximum normalizes the deconvolved signal.

Another issue that needs to be addressed is the fact that the length of the signature changes as the speed of the vehicle changes. Faster the vehicles have shorter the signatures as compared to the same vehicle driven at a slower speed. The length of the signature also depends on the length of the car. Hence the signature of a small car driven at a slow speed may have the same length as that of a longer car driven at a higher speed. This ambiguity needs to be resolved by using resampling and filtering to achieve length normalization. This issue of speed normalization is discussed further in section 5.4.

4.5 Feature Extraction

The signatures obtained after deconvolution disclose more details as compared to the unprocessed waveform, which is a smooth signal. These details such as number of peaks and valleys, their relative positions and heights give the signature a characteristic shape. The feature extraction employed in this thesis is to find the number of peaks and valleys for all the signatures, since they are the defining features of the signature.

4.6 Vehicle Reidentification

To find the matching signature, first the likely matching signatures need to be identified. This can be done by calculating a probable window of the time during which the vehicle will reach the downstream detector. This is computed using the speed estimate at the upstream detector and the distance between the two detectors. All the signatures in this window are considered the likely matches.

Various methods were tried out for matching the signatures. The signature whose match is to be found out was moved over the likely matches and the correlation coefficient was calculated at every point. The point where the correlation coefficient achieves the peak was expected to be the point of matching. This method however did not give satisfactory result since although the correlation coefficient is normalized for changes in amplitude, obtaining normalization for changes in size was difficult. The other method used for matching involves moving the signature over likely matches and finding the difference between the two.

Denote the N possible candidates of segmented matching signatures as $Y_i(t)$, $i=1, \dots, N$. The signal of the candidate signature i extends from t_i to $t_i + l(Y_i) - 1$ where $l(Y_i)$ is the length of the signature. Let the reference signature be denoted $X(t)$ and the signal extends from 0 to $l(X) - 1$ where $l(X)$ is the length of the signal supporting area. $X(t)$ is moved over $Y_i(t)$ and the difference coefficient is calculated using the following equation for every point s ,

$$\gamma_i(t_i + s) = \frac{\sum_{t=t_i}^{t_i+s} |Y_i(t) - \bar{Y}_i| - |X(t + l(X) - s - t_i) - \bar{X}|}{s + 1} \quad (26)$$

where s goes from 0 to $l(Y_i)$, \bar{Y}_i denotes the mean of $Y_i(t)$ and \bar{X} denotes the mean of $X(t)$. The position $t_i + s$ for which $\gamma_i(t_i + s)$ is minimum is considered the matching point for that probable match and is used later to estimate the travel time.

For every probable match, the overall difference coefficient is calculated as the summation of the minimum difference coefficient (given by Eq. 26), difference of number of valleys and difference between number of peaks of the probable match and the

signature to be matched. The overall matching score for a signature i with any of the probable matches j is given by:

$$\Delta_j = |\min_s [\gamma_j(t_j + s)]| + |Peaks(i) - Peaks(j)| + |Valleys(i) - Valleys(j)| \quad (27)$$

The matching signature is the one for which this matching score is minimum and the vehicle is claimed as the identified vehicle.

4.7 Travel Time estimation for individual vehicles

After the two signatures have been identified as matching signatures (signatures of the same vehicle), the next step is to decide the point in time where maximum similarity shows. This step is necessary to decide which time stamp for each channel should be considered for calculating the travel time. Few methods for this purpose are listed below.

1. Time interval between points where the signatures cross the 10% threshold
2. Time interval between points where the signatures drop below the 10% threshold
3. Time interval between 50% point of both the signatures
4. Time interval between the maximum peaks of both the signatures
5. Time interval between the points where difference coefficient is minimum

According to the tests we conducted, we found that the last method (5) gave the best results since the difference coefficient is minimum at the point where the signatures show maximum similarity. First, the signature to be matched is moved over the matching signature and the position S_1 where the difference coefficient (given by Eq 26) is minimum is determined. Then, the matching signature is moved over the signature to be matched and the position S_2 where the difference coefficient (given by Eq 26) is minimum is determined. The travel time is then estimated as the difference between the time stamps given by position S_1 and S_2 .

4.8 Travel Time Estimation from Group of Vehicles

The accuracy of the individual vehicle reidentification rate is not likely to reach 100% even if the algorithm works perfect, since two or more identical vehicle types from the same manufacture could pass over the detection zone. Suppose that we were not able to identify individual vehicles but a group of vehicles. More specifically, the arrival time of each vehicle in a group was recorded at the upstream of the highway section, but we could not match vehicles one-to-one at the downstream detector zone. However, the group was identified, and the arrival time of individual vehicles at the downstream detector station were recorded. Under this condition, we wish to identify the travel time of the group of vehicles, which should be equivalent to the average travel time of the individual vehicles. This travel time is referred to as the group travel time.

Consider that the timestamps recorded at the upstream station are F_i (for $i= 1$ to n) and the timestamps at the downstream station are S_i (for $i = 1$ to m), where n is the number of vehicles in the group at the upstream station and m is the number of vehicles in the group at the downstream station. Notice that m and n may not be equal since we cannot guarantee that the vehicle groups will retain their structure as they pass from one station to another.

There can be a number of ways to compute the average time taken by a vehicle belonging to a group to travel from the upstream station to the downstream station. Below discusses four computational examples of group travel time.

1. The basic idea behind this approach is that the vehicle at the i^{th} position at the upstream station can be at any j^{th} ($j = 0$ to m) position when the group reaches the downstream station. The travel time T_i for the i^{th} vehicle at the upstream station can be estimated as

$$T_i = \frac{\sum_{j=1}^m (S_j - F_i)}{m} \quad (28)$$

Hence, the average travel time taken for the entire group to travel from the upstream station to the downstream station is given by

$$GroupTravelTime = \frac{\sum_{i=1}^n T_i}{n} \quad (29)$$

2. A group of vehicles may be treated as a single entity. The group travel time then can be estimated the difference between the average of the timestamp of arrival at the upstream station and the average of the timestamps of arrival at the downstream station, i.e.,

$$GroupTravelTime = \frac{1}{m} \sum_{j=1}^m S_j - \frac{1}{n} \sum_{i=1}^n F_i \quad (30)$$

3. Instead of finding the average of all the arrival timestamps, only the average of the head and tail of the group may be taken to simplify the computation.

$$GroupTravelTime = \frac{(S_1 + S_m)}{2} - \frac{(F_1 + F_n)}{2} \quad (31)$$

This method is considered less reliable than previous two since it is prone to be influenced by outliers.

4. The problem with all of the above approaches is that they do not take into account the outliers. Hence, a more robust way would be to remove the outliers from the group before calculating the group. Various tests and algorithms can be used to detect the outliers. One simple way to detect outliers is to compare the absolute difference between the sample and the median to a threshold. After removing the outliers, the first and second method can be used to compute the group travel time.

5 EXPERIMENTAL RESULTS

5.1 Data collection

5.1.1 Highway data

For this research, the ILD waveform data was mainly collected from the 3M-research site near the I-35W/I-94 intersection in Minneapolis. This site contains many different types of loop installations for testing the effectiveness of loop configuration. The data was collected in pairs of loop detectors, one from an upstream location and the other from a downstream location with 60 ft apart. Since both loops are terminated at the same control cabinet, we were able to collect data in a single file with synchronized time. The types of loop cards used are Canoga C800 series. The change in inductance was recorded approximately at every 10 ms along with a time stamp. The loop detector cabinet and laptop PC setup used for data collection are shown in Figure 7. Data was captured by connecting the communication port of Canoga card and the laptop computers.

In addition, for verification of vehicle identification, a high-speed video recording system was used to record the vehicles passing the detector along with a time stamp. 3M Company specifically designed this video system to synchronize with loop detector actuation and millisecond time stamps. For our experiments, this video recording was used for visual verification of reidentification.

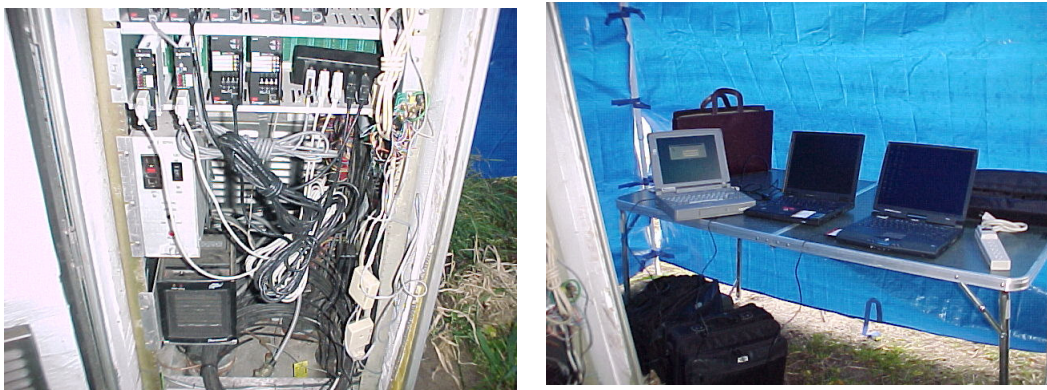


Figure 7: Data collection equipment: left=detector cabinet, right=laptop computers



Figure 8: Video recording system with loop actuation and timestamp

5.1.2 Data collection for impulse response of loop system

An attempt was also made to collect data to estimate the impulse response of the loop system. For this purpose, a steel pipe fitted with two wheels at both ends was moved over the loop and the change in inductance was recorded (Figure 9). The idea was that as the pipe cuts the flux of the loop, there would be a change in inductance, which will be very close to the impulse response of the ILD system, assuming the steel pipe acts as an impulse input. However due to limited metal surface of the pipe and the low sensitivity of the inductance loop, the data failed to show any changes in inductance when the pipe was moved over the loop.



Figure 9: Apparatus used for loop system impulse response

A better approach of creating impulse input could have been using a vertical sheet of steel to create a large surface to form sufficient amount of eddy currents. This attempt was not made due to the difficulty of building such object and insufficient resources. It was also uncertain that movement of a large sheet would work as an impulse input or not. We conclude that finding the impulse response of an ILD system using a physical input is difficult since it must be a 3-dimensional physical input. Thus, we still do not know what precisely the impulse input should be and decided to leave the ILD system as a blind system.

5.1.3 Waveforms on different speeds of the same vehicle

In order to check the ability of the algorithm to match signatures collected at different speed, a set inductive waveforms of the same car at different speeds was collected. For this purpose, inductive waveforms for a Ford Ranger (Axle Length =10' 5.7" and Height=1' 9") were collected at four different speeds (10mph, 20mph, 30mph, 39mph). The vehicle crossing the loop we measured is shown in Figure 10.



Figure 10: Ford Ranger used to collect inductance waveforms at various speeds

5.2 Deconvolution Examples

5.2.1 Effect of deconvolution

The effect of deconvolution is demonstrated using two inductance waveforms of passenger vehicles. The data used for this portion was collected from the 3M loop research site. The data is organized as two channels in which the first channel is the data stream recorded from the upstream station and the second channel is the data stream recorded from the downstream station. The waveforms of two vehicles used in this example are shown in Figure 11. In the graph, the data from the upstream station was depicted as a solid line (Ch0) and the data from the downstream station was depicted as a dotted line (Ch1). Thus, the first pair of solid and dotted waveforms is the first vehicle and the second pair solid and dotted waveforms are the second vehicle. It can be clearly noticed from the graph that the waveforms are extremely smooth indicating the effect of loop convolution effect. From this graph, we can deduce that the ILD system function is a smoothing function such as a square or the function described in Section 3.4.

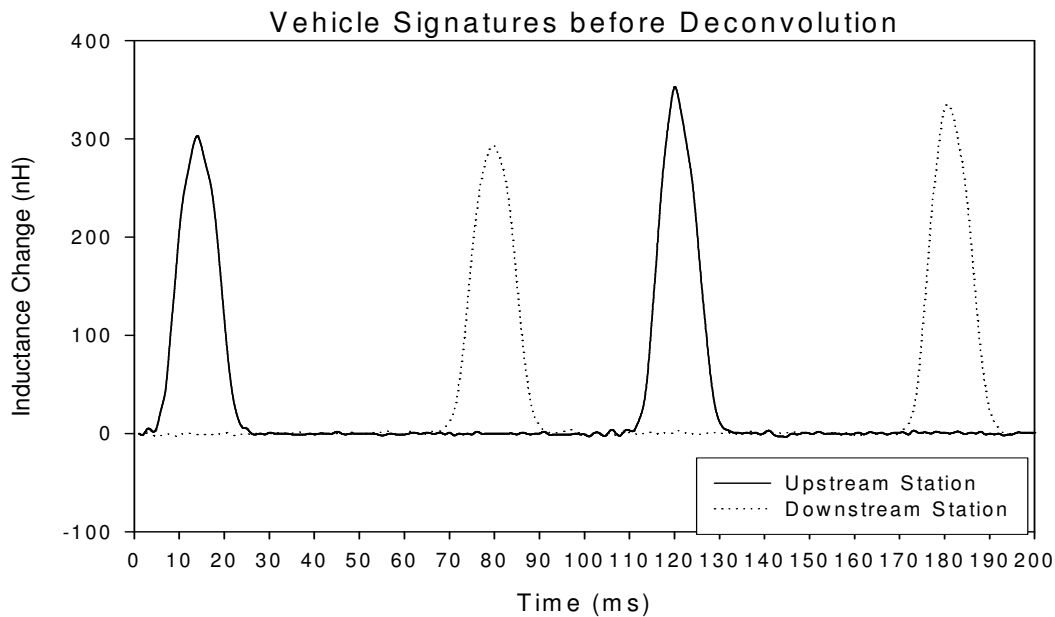


Figure 11: Inductance waveform of two passenger vehicles recorded in two separate stations

We now show the effect of deconvolution. The inductance waveforms in Figure 11 are processed using Eq. (16) with H designed as a simple rounded square wave in time domain. For computation, 256 FFT and IFFT were used. The result is shown in Figure 12. Notice from the waveforms that the details are recovered from the smoothed signal showing the differences in the basic shape. Before the deconvolution, all of the four signatures had very similar shape characteristics, so it was very difficult to discriminate between them. Figure 12 now clearly shows the differences between the two vehicles, which can be used as vehicle features or signatures. The first vehicle can be characterized as two peaks with equal height, and the second pair can be characterized one higher first peak and a shorter second peak. These distinguishable characteristics lead to a higher rate of vehicle reidentification. However, the deconvolution process also adds noise on the channel, so a filtering is required after the deconvolution.

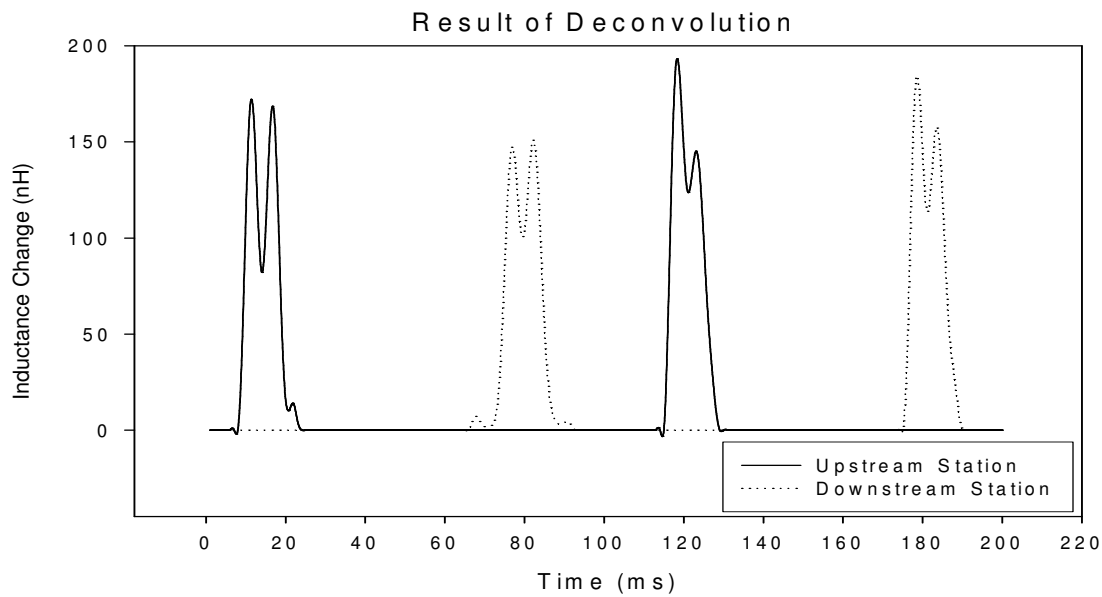


Figure 12: Result of deconvolution

5.2.2 Comparison example of three vehicles in similar length

The raw inductance waveforms show only minute differences as long as the vehicle length is similar. Figure 13 shows three vehicles of completely different types and their waveforms along with the video images. In the graph, the solid line shows the raw inductance waveform before deconvolution and the dotted line shows the signature obtained after the deconvolution. Notice that all three solid line signatures have a similar shape and do not expose clearly distinguishable features, even though the vehicles are completely different. Now notice the signatures obtained after the deconvolution, i.e. the dotted lines. It clearly shows distinguishable features that can be characterized by peak and valley types.

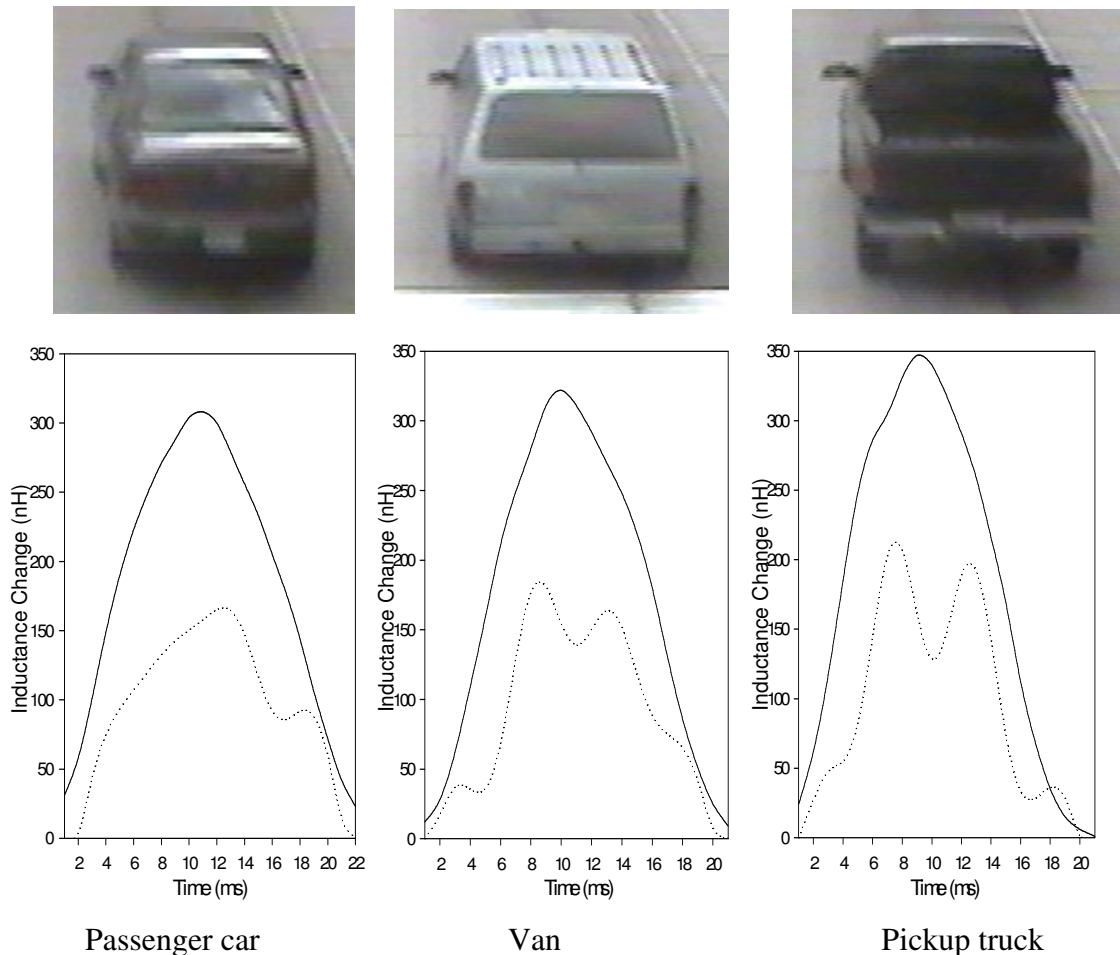


Figure 13: Comparison of vehicle with a similar length

5.2.3 Comparison example of three vehicles with the same type

In order to answer the question on how the deconvolution would perform if the vehicles are in the same class, we selected three passenger cars. Figure 14 shows three different passenger cars and their waveforms. Again, the vehicle waveforms before deconvolution are shown in solid lines and, after deconvolution, is shown in dotted lines. The top row images are the corresponding vehicles. These vehicles were traveling around 68 mph. It can be clearly seen that all three solid line signatures have a similar shape and characteristics and fail to provide any discriminating information about the vehicles. On the other hand, the waveforms obtained after deconvolution clearly show different shapes for all three vehicles. More specifically, the number of peaks and valleys, and the sizes are clearly distinguishable. The deconvolution was performed using Eq. 16 with a static model of H function (a smooth square function).

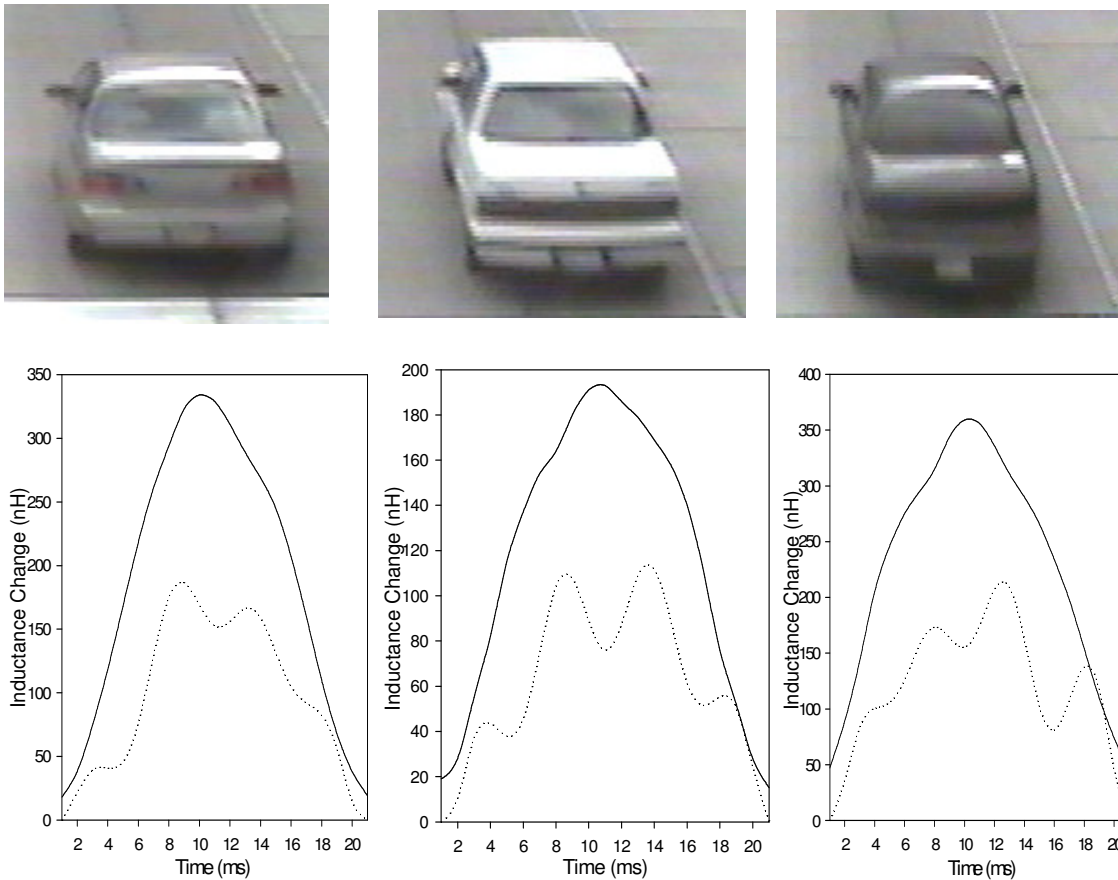


Figure 14: Comparison of three passenger car vehicles: before deconvolution=solid line, after deconvolution=dotted line

5.2.4 Reidentification Example-1

This example illustrates a reidentification example based on deconvolved waveforms. Figure 16 shows vehicle signatures before (shown by solid line) and after deconvolution (shown by dotted line). The upstream signature shown in (a) is compared with three downstream signatures (b)-(d). The matching scores are (b)=10, (c)=25, (d)=17, so the minimum is the downstream signature (b). Hence, the upstream signature (a) is matched to downstream signature (b). This is correct and is verified by the vehicle images.

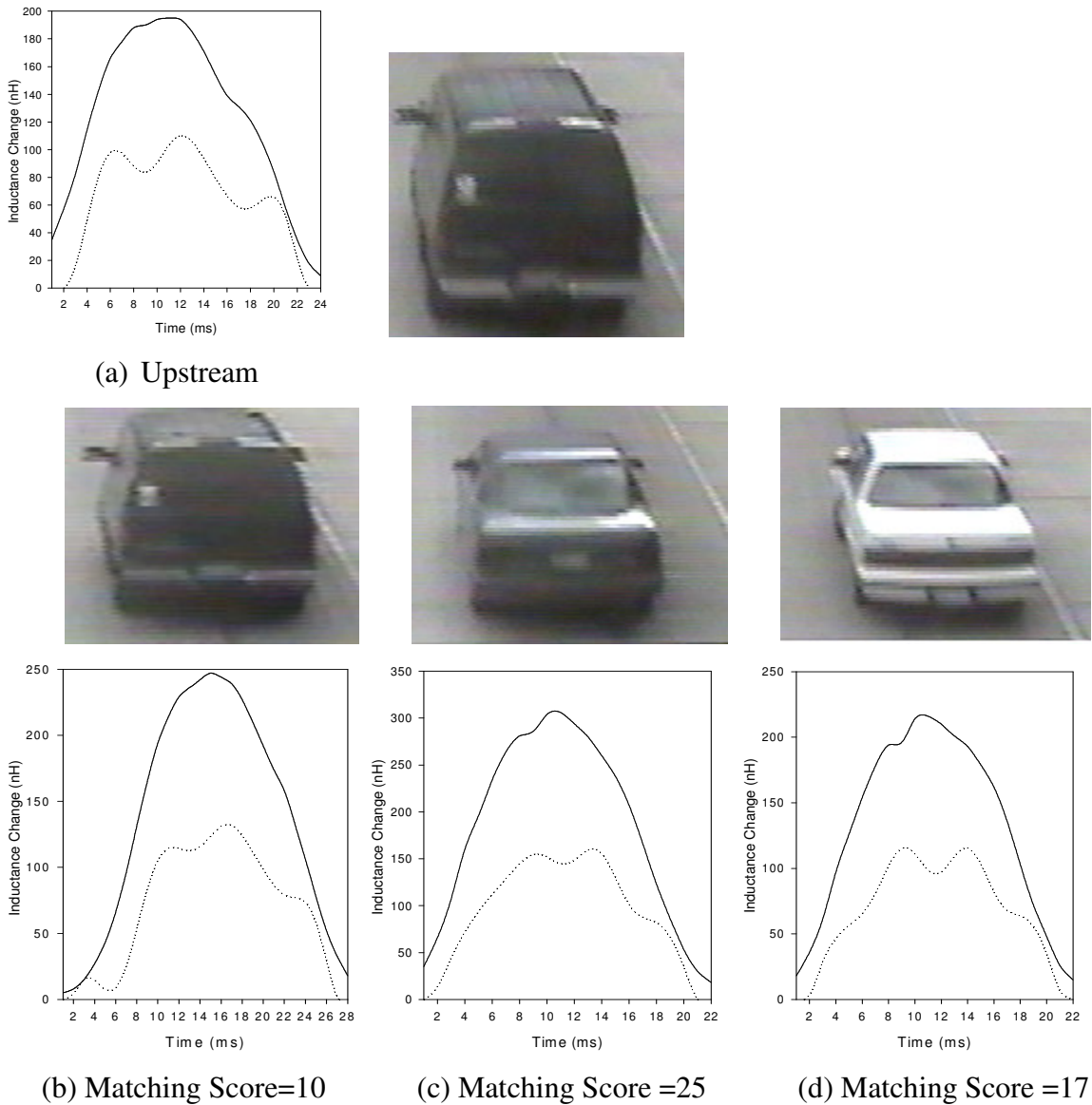


Figure 15: Vehicle reidentification. (a) is the upstream vehicle, and (b)-(d) are possible match candidates at the downstream vehicles. (Before deconvolution=solid, after deconvolution=dotted).

5.2.5 Reidentification Example-2

This example illustrates the second reidentification example that was failed when we use only simple difference coefficients. The waveforms before and after deconvolution are illustrated in Figure 17. The upstream signature is compared with three downstream signatures (b)-(d). The matching scores are (b)=14, (c)=12, (d)=22, so the minimum is the downstream signature (c). Hence, the upstream signature (a) is matched to the downstream signature (c). However, the correct match in this case is (b). For verification, see the images shown in Figure 16. In this case, the reidentification algorithm was not successful in finding the correct match.

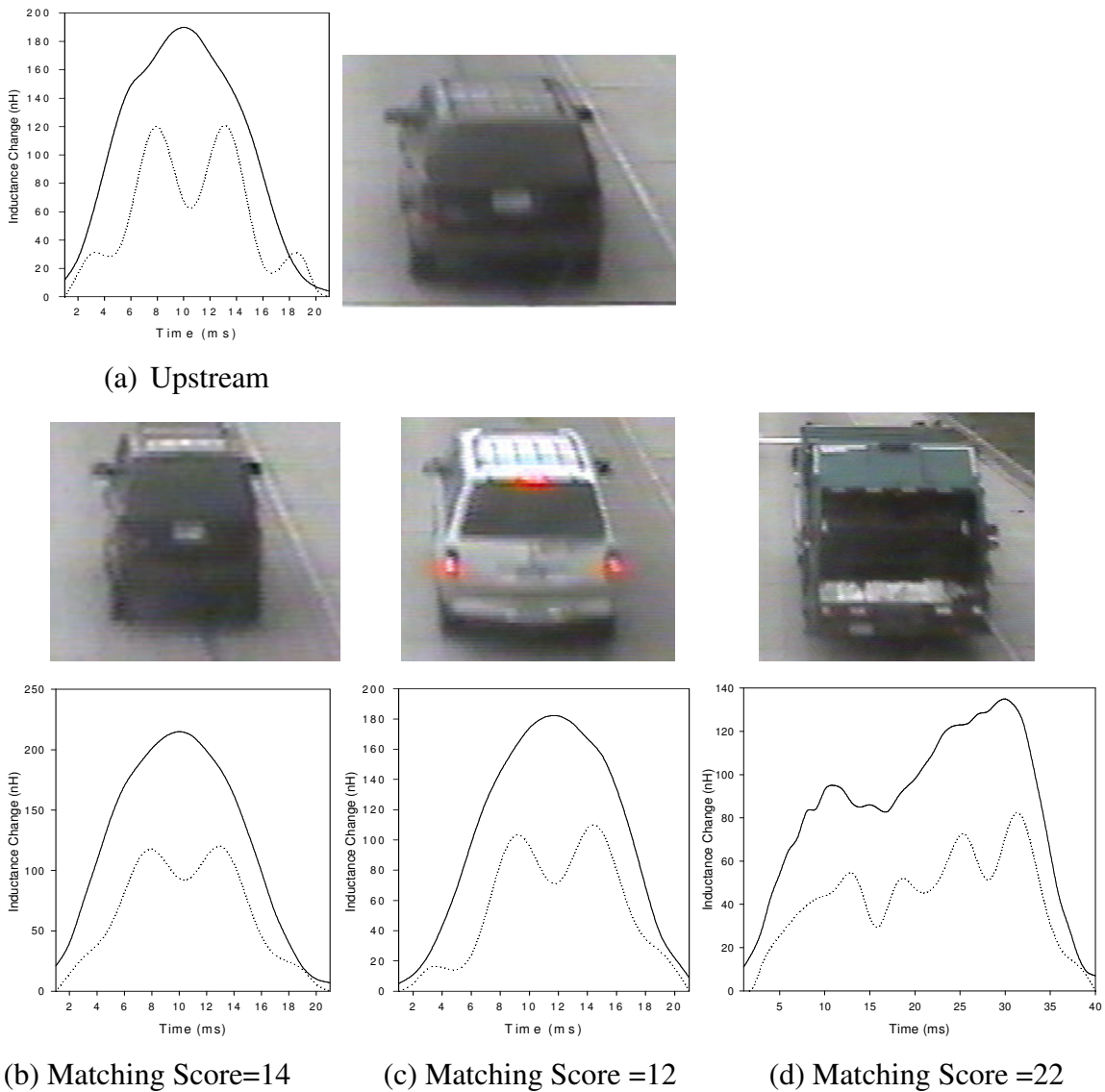


Figure 16: Vehicle reidentification. (a) is the upstream vehicle, and (b)-(d) are possible match candidates at the downstream vehicles. (Before deconvolution=solid, after deconvolution=dotted).

5.3 Godard Blind Deconvolution Examples

This sub-section repeats examples for the Godard blind deconvolution.

5.3.1 Comparison example of three vehicles in similar length

Figure 17 shows three vehicles of different types and their signatures. The vehicle signature before Godard blind deconvolution is shown by solid line and the signatures obtained after Godard deconvolution by dotted line. It can be seen that all three solid lined waveforms have similar shape and fail to provide detailed information about the vehicle. However, the waveforms obtained after Godard blind deconvolution show the features that are more distinctive. This greatly aids in the task of matching vehicles.

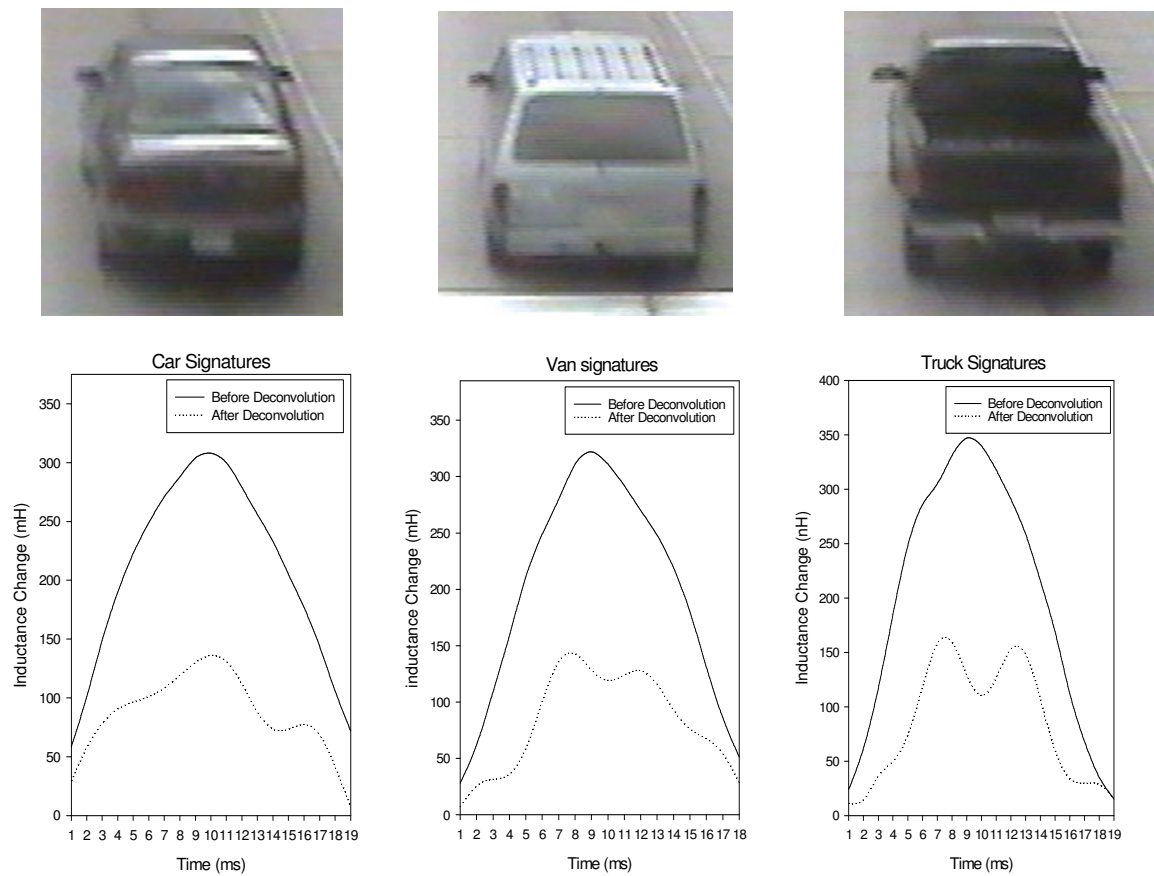


Figure 17: Comparison of vehicle waveforms with a similar length before and after Godard blind deconvolution. The three vehicles are a car, a van, and a pick-up truck.

5.3.2 Comparison example of three passenger car vehicles

Figure 18 shows three different passenger cars and their signatures. The vehicle signature before Godard blind deconvolution is shown in red while the signature obtained after deconvolution is in green. It can be seen that all three red signatures have similar shape and fail to provide any discriminating information about the vehicle. However the signatures obtained after Godard blind deconvolution show different shapes for all three vehicles. This characteristic shape of each individual vehicle is used to achieve accurate re-identification.

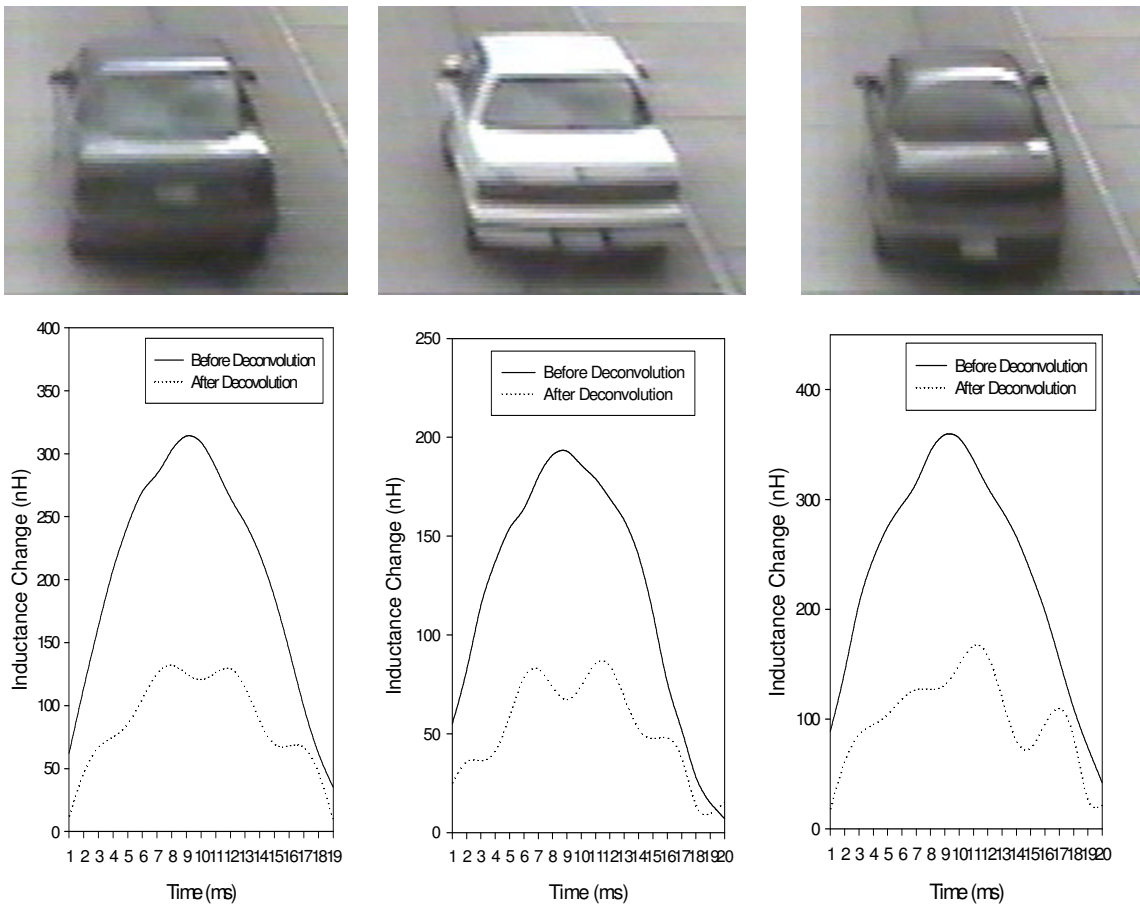


Figure 18: Comparison of three passenger car vehicles on before and after deconvolution: before=solid, after=dotted

5.3.3 Reidentification Example-1

This example illustrates reidentification based on Godard deconvolution. Figure 19 shows the vehicle signatures before (shown by solid line) and after (shown by dotted) Godard deconvolution. The upstream signature shown in (a) is compared with three downstream signatures (b)-(d). The matching scores are (b)=12, (c)=27, (d)=29, so the minimum in this case is the downstream signature (b). Hence, the upstream signature (a) is matched to downstream signature (b). This is correct and verified based on the vehicle images (see Figure 19).

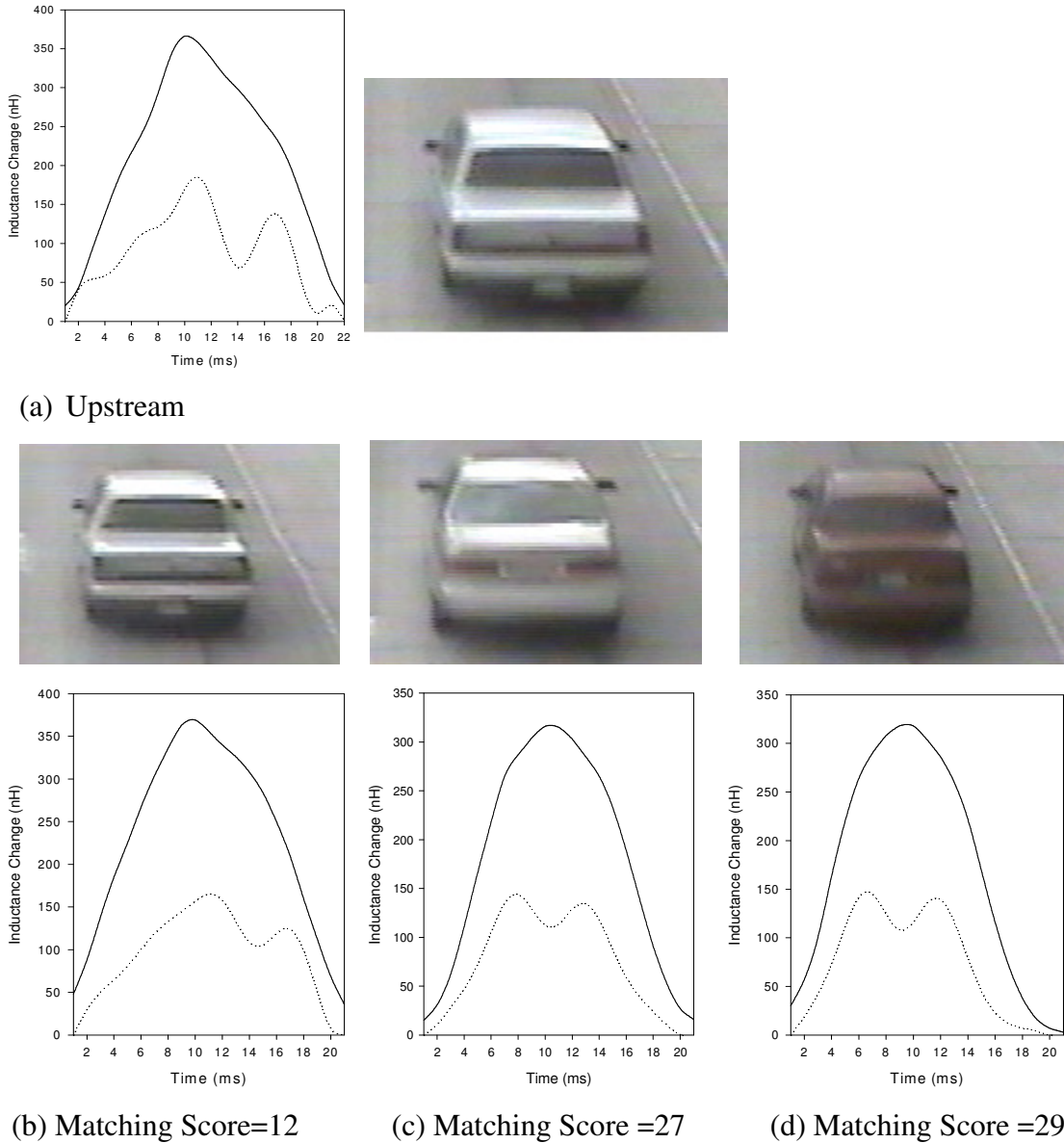


Figure 19: Vehicle reidentification. (a) is the upstream vehicle, and (b)-(d) are possible match candidates at the downstream vehicles. (Before deconvolution=solid, after deconvolution=dotted).

5.3.3 Reidentification Example-2

This example illustrates the second reidentification example that was failed when we use only simple difference coefficients. The waveforms before and after Godard deconvolution are illustrated in Figure 21. The upstream signature is compared with three downstream signatures (b)-(d). The matching scores are (b)=12, (c)=17, (d)=11, so the minimum is the downstream signature (c). Hence, the upstream signature (a) is matched to the downstream signature (c). However, the correct match in this case is (b). For verification, see the images shown in Figure 20. In this case, the reidentification algorithm was not successful in finding the correct match.

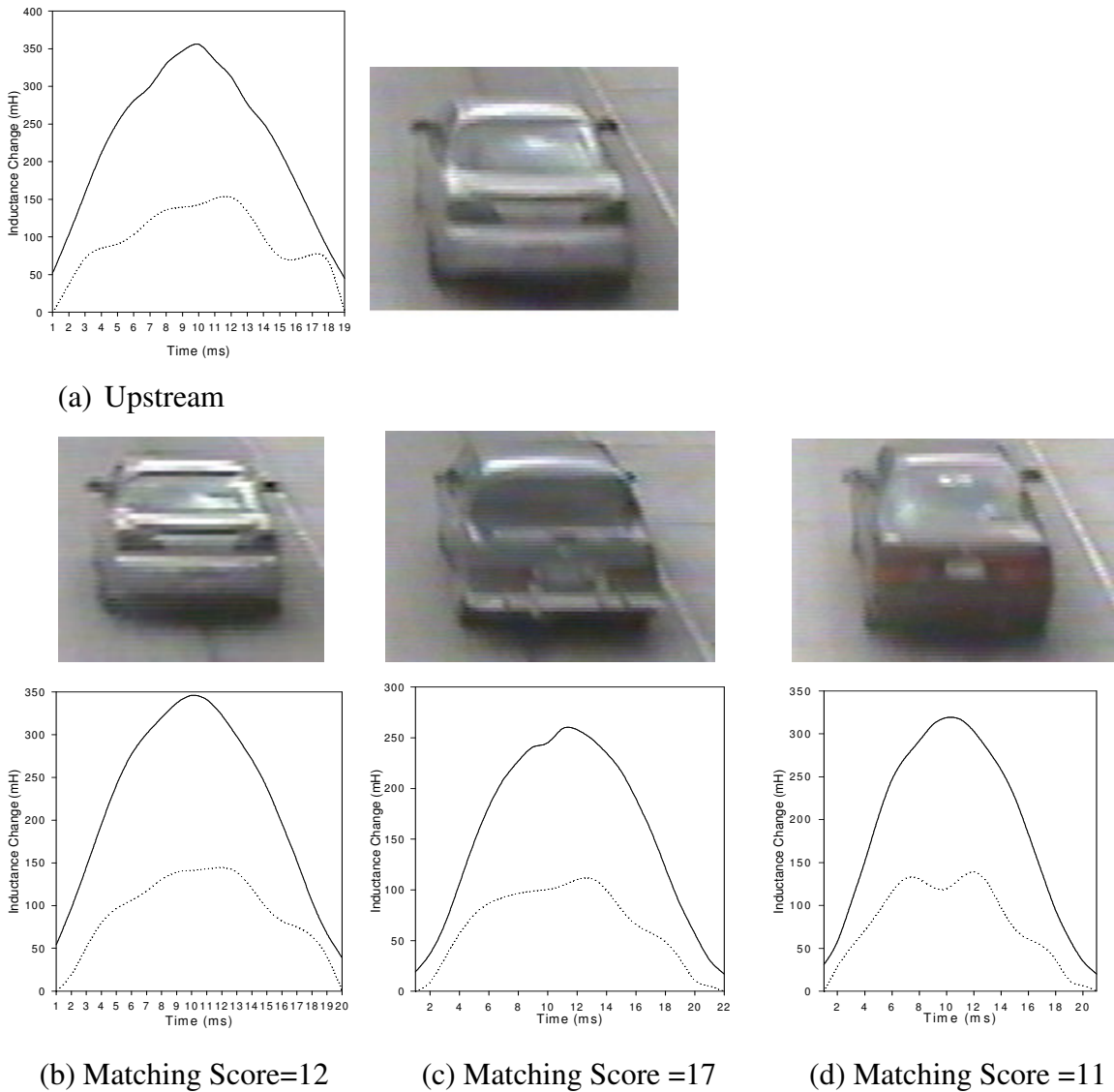


Figure 20: Vehicle reidentification. (a) is the upstream vehicle, and (b)-(d) are possible match candidates at the downstream vehicles. (Before deconvolution=solid, after deconvolution=dotted).

5.4 Speed Normalization

As mentioned in Section 3, the length of the inductance waveforms not only depends on the length of the vehicle but also on the speed of the vehicle. The effect of speed and the related normalization techniques are discussed. In Figures 21 and 22, the dotted line represents the raw inductance signatures for the same vehicle driven at 10 mph and 39 mph respectively. This data was taken using a Ford Ranger as described in Section 5.1.3. Note that the length of the signature in Figure 21 (10 mph) is nearly four times that of in Figure 22 (39 mph), since the speed ratio is four. This means that some kind of speed normalization will be required to make the signatures characteristic to the vehicle irrespective of the speed.

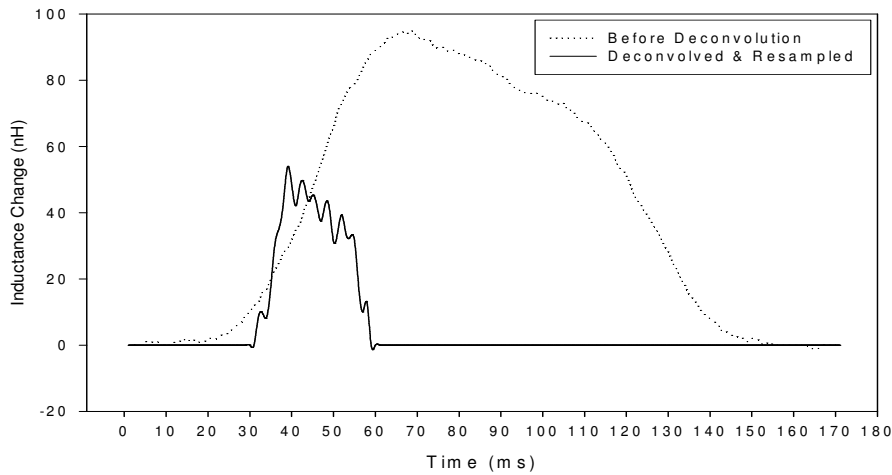


Figure 21: Original (dotted) and deconvolved and then resampled (solid) signature of Ford Ranger driven at 10mph

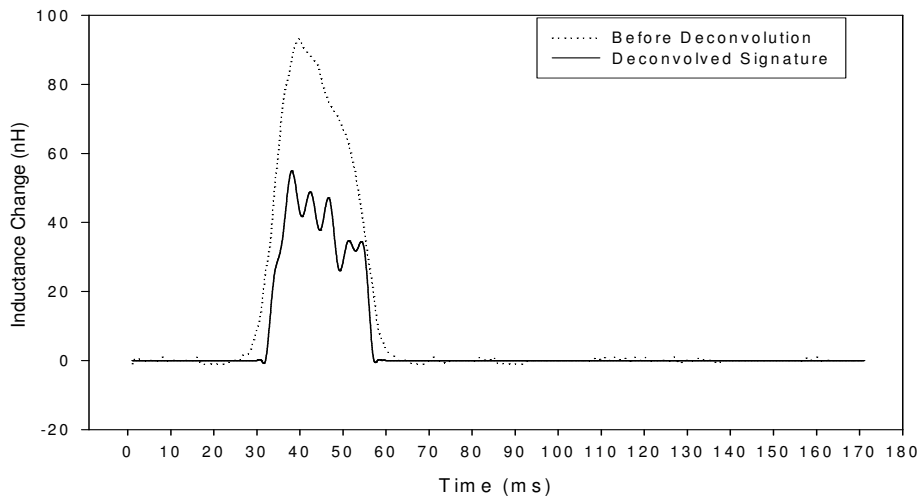


Figure 22: Original (dotted) and deconvolved (solid) signature of Ford Ranger driven at 39mph.

A simple but effective approach is to normalize the vehicle signature to a length equal to the length of the shortest signature (fastest speed). The idea behind this approach is that since the shortest signature contains least information, the other signatures are time normalized to the shortest. To this end, we first compute the sample ratio k by,

$$k = \frac{\text{No of samples of comparing signature}}{\text{No of samples in the shortest signature}} \quad (29)$$

The first method devised to convert to a normalized waveform was to compute the new samples by averaging k samples. In all, M new samples are computed where M is the number of samples in the shortest signature. Hence, the new signature obtained has the same length as the shortest signature, providing the same length for different speeds.

The second method devised was to resample the longer signatures to the shortest length. As shown in Figure 24 block diagram, the deconvolved signature is first passed through a low pass filter in order to remove high-frequency components. This low pass filter is designed with a cutoff frequency of ω given by,

$$\omega = \frac{(0.5\pi)}{k} \quad (30)$$

The filtered signature is then down-sampled by taking every k^{th} sample. However, if k is a fraction then linear interpolation is used to find the value of the sample at $n*k$ (where $n=1,2,\dots,M$).

Experimental results show that the resampled low speed signature retains the pattern characteristics of the higher speed signature. In Figure 22, the solid line waveform is the resampled signature obtained when the speed of 10 mph was normalized to 39 mph. The solid line waveform in Figure 23 is the deconvolved signature at the speed of 39 mph. Both signatures show similar peak pattern with little differences in the relative height of the peaks. The resampled signature also shows two irregularities at the beginning of the leading edge and at the end of the trailing edge. These can be attributed to the non-uniform speed while passing over the loop since it is extremely difficult to keep the speed constant at 10 mph. However it is much simpler to keep the speed uniform at a higher speed, hence these irregularities are absent in the 39 mph signature. As

demonstrated by this example, speed normalization can be used to obtain deconvolved signatures that are speed independent.

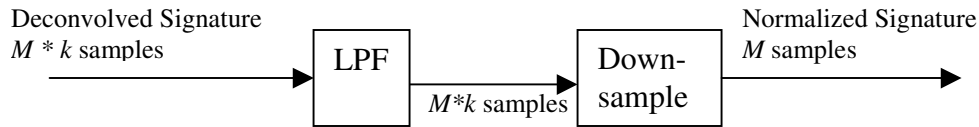


Figure 23: Speed normalization down-sampling

5.5 Real time implementation aspects

In real time applications, the computation time between arrivals of vehicle waveforms is extremely vital. The success of a system depends on whether the computation time is enough to do the work in real time or not. In case of real time implementation, we need to consider that the road will have more than one lane and the distance between the upstream and downstream loops can be in miles. Hence, the system will have to compare each signature to a large number of signatures in order to find the correct match. Apart from matching, the blind deconvolution process requires filtering, which takes significant time. If we consider our 3M test data "Test1.txt", the deconvolution for 560 signatures takes a time of 5.43 seconds (10 ms per signature) and the time taken for matching is 0.29 seconds for 560 signatures, which is considerably less as compared to deconvolution. Hence, to process a single signature and compare it with 50 other signature will take approx half a second (time to deconvolve 50 signatures).

Another important aspect of the real time implementation is having a communication channel between the upstream and the downstream station to send the signatures as they arrive. A memory buffer is also needed to store signatures before processing. Data recorded from two channels for an hour from a single lane road amount to the size of 4000 KB. The size of the buffer needed depends on the number of lanes the road has, the traffic intensity and the time needed for computation.

5.6 Overall performance of reidentification

During the data collection process, we collected two large data sets named “Test1.txt” and “Test2.txt”. Table 2 summarizes the overall performance of our approaches, which include various computational steps, number of vehicles and the reidentification rate. Note that for the test file Test1.txt, even though the reidentification rate is slightly higher when Godard blind deconvolution technique is used, the computation time needed is more than 70 times as compared to CLS deconvolution. The identification rate of Godard deconvolution was less in the data Test2.txt.

Table 2: Performance results of the 3M test data

Method	CLS Deconvolution		Godard Blind Deconvolution	
	Test1.txt	Test2.txt	Test1.txt	Test2.txt
No. Of Signatures	563	760	563	760
File Size	1533 KB	4030 KB	1533 KB	4030 KB
Splitting time	1.315 sec	1.641 sec	1.188 sec	1.578 sec
Filtering Time	5.516 sec	7.172 sec	401.672 sec	660.375 sec
Feature Extraction Time	0.047 sec	0.047 sec	0.031 sec	0.031 sec
Matching Time	0.234 sec	0.313 sec	0.203 sec	0.344 sec
Re-identification Rate	89.88%	88.82%	90.05%	85.92%

The reidentification algorithm was also run for the raw vehicle waveforms (before deconvolution) to compare the identification rates against the deconvolved waveforms. Table 3 summarizes the reidentification rates obtained before and after deconvolution. In the table, “the difference coefficient threshold” indicates the ceiling value of the difference coefficient that the correct match should not exceed. If the difference coefficient of the matching signature were greater than this threshold, then the algorithm declares that sufficient similarities do not exist to claim re-identification. Hence, the threshold on the difference coefficient provides a way to eliminate those cases where reidentification is marginal. In summary, the data set, test1.txt, achieved higher reidentification rates after deconvolution, while no significant improvements were observed for the data set, Text2.txt on the matching test with a difference-coefficient threshold.

Table 3: Re-identification rates for the 3M test data with threshold on the difference coefficient

Difference Coefficient Threshold	Without Deconvolution		CLS Deconvolution		Godard Blind Deconvolution	
	Test1.txt	Test2.txt	Test1.txt	Test2.txt	Test1.txt	Test2.txt
13	56.13	89.87	74.25	88.42	87.39	85.39
15	73.16	89.87	82.24	88.62	88.81	85.79
17	82.42	89.87	86.32	88.82	89.88	85.79
19	86.5	89.87	87.74	88.82	89.88	85.92

6 CONCLUSIONS AND RECOMMENDATIONS

6.1 Conclusions

The thesis presented a deconvolution approach that significantly enhances the features of vehicle inductance signature. The underlying theory behind deconvolution is that, since the features are lost by a convolution process in the ILD systems, a deconvolution process would be able to reverse the process providing more unique features for each vehicle. The deconvolution filter was estimated using two methods, namely the Godard blind deconvolution technique and CLS filter based on estimates of loop characteristic function.

The advantage of Godard technique lies in the fact that it converges to a good solution, if the algorithm starts from a rough estimate of the ILD impulse response. The cost that is paid is the higher computational time needed to perform the numerous iterations. The CLS filter performance seems similar as long as a reasonable estimate of loop characteristic function is used, which we achieved by using a modeling of the ILD impulse response.

To verify the theory, we conducted various experiments and found significant improvements in features in all cases. Based on the theory and experimental results, we are confident to conclude that deconvolved signal exposes more unique vehicle features than the signals without deconvolution. This result not only helps improve the accuracy of travel time measurements but also helps other applications such as a vehicle classification or tracking that could be developed based on vehicle inductance signatures .

6.2 Future Recommendations

Although the blind deconvolution techniques implemented in this thesis yielded satisfactory results, other deconvolution techniques based on information theoretic model or higher order statistics can be tried out and compared with the techniques used in this thesis to further the study to find the most effective deconvolution method. The speed estimation method used in the thesis is a very straightforward method. However, the accuracy with which the speed is estimated depends on the accurate estimation of the

vehicle length. Other methods that can estimate speed independent of the vehicle length can be further explored.

This thesis describes the need as well as the technique to achieve speed normalization. However, speed normalization was not implemented for the 3M data. Future work can include speed normalization for all the signatures to make re-identification more accurate.

Another way to obtain higher re-identification rates would be to develop better feature extraction and pattern matching techniques. This thesis only explored the very basic level, and more advanced pattern recognition techniques should be explored.

The next steps of this research would be to directly implement the developed technology in a section of highway using a pair of spatially separated detector stations and verify the accuracy of travel time measurements using a cell-phone probe. This step would require implementation of a communication network and redesign of algorithm steps to meet the real-time requirements.

REFERENCES

Bell, A. J., Sejnowski, T. (1995), "Blind separation and blind deconvolution: an information-theoretic approach," Proc. ICASSP, (Detroit), 1995.

Coifman, B. (2000), "New Aggregation Strategies to Improve Velocity Estimation From Single Loop Detectors," California PATH Paper, UCB-ITS-PWP-2000-12.

Dailey, D. (1999), "A Statistical Algorithm for Estimating Speed from Single Loop Volume and Occupancy Measurement," TRB, Vol 33B, No 5, June 1999, pp 313-322.

Feng, C., Chi, C. (1999), "Performance of cumulant based inverse filters for blind Deconvolution," IEEE Transactions on Signal Processing, Volume 47 Issue 7, (1922-1935), July 1999.

Godard D.N. (1980), "Self-recovering equalization and carrier tracking in a two-dimensional data communication systems," IEEE Transactions on Communications, Volume 28, (1867-1875), 1980.

Gonzalez, R.C., & Woods, R. E. (1993) "Digital Image Processing", Addison-Wesley, Reading, Massachusetts, 1993.

Gray, R.M. (1990), "Entropy and information theory"

<http://www-ee.stanford.edu/~gray/it.pdf>

Haykin, S. (2000), "Unsupervised adaptive filtering Volume 2: Blind deconvolution," Wiley Inter-Science Publication, April 2000.

Johnson, R.C., Schniter, P., Endres, T.J., Behm, J.D., Brown, D.R., Casas, R.A. (1998), "Blind equalization using the constant modulus criterion: a review," Proceedings of the IEEE, October 1998.

Khan, S and Thanasupsin K (2000), "Estimating Link Travel Time on I-70 Corridor: A Real- Time Demonstration Prototype" by Colorado Department of Transportation, Research Branch, 4201 East Arkansas Avenue, Denver CO 80222; ph. (303) 757-9506; <http://www.dot.state.co.us>) [TD100:CO00-15]

Lee, W., Cheun, K. (1999), "Convergence analysis of the stop-and-go blind equalization algorithm," IEEE transactions on communications, Volume 47, No 2, February 1999.

Lucky, R.W. (1966), "Techniques for adaptive equalisation of digital communication systems," Bell System Tech. J., Volume 45,(255-286), 1966.

Mathis, H., Douglas S.C. (2003), "Blind deconvolution of impulsive signals using a modified Sato algorithm," Signal Processing, IEEE Transactions on Signal Processing, Volume 51, Issue 7, (1905 -1915), July 2003 .

Mendel, J.M. (1991), "Tutorial on higher-order statistics (spectra) in signal processing and system theory: Theoretical results and some applications," Proceedings of the IEEE, Volume 79, No 3, March 1991.

Mikhalkin, B., Payne, H., Isaksen, L. (1972), "Estimation of Speed from Presence Detectors," Highway Research Record 388, pp 73-83. Highway Research Board, Washington, DC.

Nokas, G., Dermatas, E., Kokkinakis, G. (1998), "Robust speech recognition in noisy reverberant rooms," Workshop on text, speech and dialogue Pilsen, Czech Republic, September, 1998.

Nowlan, S.J., & Hinton, G.E. (1993), "A Soft Decision-Directed LMS algorithm for blind equalization," IEEE Transactions on communications, Volume 41, No 2, Feb1993.

Olofsson, T., Stepinski, T. (1996), "Blind deconvolution through parametric identification using second and fourth order cummulants," Ultrasonics Symposium, 1996. Proceedings of the IEEE, Volume 1, (717 -721), November 1996.

Pushkar, A., Hall, F., Acha-Daza, J. (1994), "Estimation of Speeds from Single-Loop Freeway Flow and Occupancy Data Using Cusp Catastrophe Theory Model," Transportation Research Record 1457, pp 149-157. Transportation Research Board, Washington, DC.

Sato, Y. (1975), "Two extensional applications of the zero-forcing equalization method," IEEE Transactions on Communications, Volume 42, (684-687), 1975.

Shalvi, O., Weinstein, E. (1990), "New criteria for blind deconvolution of nonminimum phase systems (channels)," IEEE transactions on information theory, Volume 36, (312-321), March 1990.

Sun, C., Ritchie, S.G. (1999), "Individual Vehicle Speed Estimation Using Single Loop Inductive Waveforms," California PATH Working Paper, October 1999.

Sun, C. (2000), "An Investigation in the Use of Inductive Loop Signatures for Vehicle Classification," California PATH Research Report, March 2000.

Sun, C., Ritchie, S.G., Park, S., Oh, C. (2002)," Field Investigation of Advanced Vehicle Reidentification Techniques and Detector Technologies – Phase 1," California PATH Research Report, March 2002.

Tam, R. (1999/2000), "PATH ATMIS: State of Research Annual Report," California PATH Paper, UCB-ITS-PWP-2000-19.

Weerackody, V., Kassam, S.A. (1994), "Dual-mode type algorithms for blind equalization," *IEEE Transactions on Communications*, Volume 41, Issue 2, (22-28), Jan 1994.

Yim. Y., Ygnace, J., Drane, C., (2000) "Travel Time Estimation on the San Francisco Bay Area Network Using Cellular Phones as Probes," California PATH Draft Report D2000-43.

Zheng, F.C., McLaughlin, S., Mulgrew, B., (1991), "Blind deconvolution algorithms based on 3rd and 4th order cummulants," *IEEE Transactions on Signal Processing*, Volume 41, Issue 2, (681 -691), February 1993.

Zervakis, M. E., & Kwon, T. M. (1992), "Robust Estimation Techniques in Regularized Image Restoration," *SPIE Optical Engineering*, vol. 31, no. 10, pp. 2174-2190, Oct. 1992.